

Dynamical Structure Factor for the Alternating Heisenberg Chain: A Linked Cluster Calculation

Chris J. Hamer^{(a)*}, Weihong Zheng^{(a)†}, and Rajiv R. P. Singh^(b)

^(a) *School of Physics, University of New South Wales, Sydney NSW 2052, Australia*

^(b) *Department of Physics, University of California, Davis, CA 95616*

(March 22, 2022)

We develop a linked cluster method to calculate the spectral weights of many-particle excitations at zero temperature. The dynamical structure factor is expressed as a sum of ‘exclusive’ structure factors, each representing contributions from a given set of excited states. A linked cluster technique to obtain high order series expansions for these quantities is discussed. We apply these methods to the alternating Heisenberg chain around the dimerized limit ($\lambda = 0$), where complete wavevector and frequency dependent spectral weights for one and two-particle excitations (continuum and bound-states) are obtained. For small to moderate values of the inter-dimer coupling parameter λ , these lead to extremely accurate calculations of the dynamical structure factors. We also examine the variation of the relative spectral weights of one and two-particle states with bond alternation all the way up to the limit of the uniform chain ($\lambda = 1$). In agreement with Schmidt and Uhrig, we find that the spectral weight is dominated by 2-triplet states even at $\lambda = 1$, which implies that a description in terms of triplet-pair excitations remains a good quantitative description of the system even for the uniform chain.

PACS numbers: 75.40.Gb, 75.10.Jm, 75.50.Ee

I. INTRODUCTION

Controlled and systematic calculation of dynamical properties of quantum lattice models remains a challenging computational task. Despite much recent progress in developing computational methods, such as the density matrix renormalization group, quantum Monte Carlo and series expansions, the dynamical properties, especially those associated with multiparticle excitations, remain poorly understood. In many systems, these multiparticle excitations have relatively small spectral weights. But in low-dimensional systems, they can become extremely important and even dominate the spectral functions. The increased frequency and wavevector resolution of various dynamical experiments, especially neutron scattering, necessitates going beyond the single-particle picture and obtaining quantitatively accurate results for the full dynamical structure factors.

One effective way to study quantum lattice models has been by using high order power series expansions in a suitable coupling constant. These methods have long been used to study ground state properties and elementary excitation spectra. Recently, they have been extended to multiparticle excitation spectra as well [1–3]. In particular, the linked cluster expansion method [4] is a particularly efficient way to carry out these calculations, which provides substantial internal checks on the validity of the expansions, and allows one to carry out the calculations by automated computer programs.

Here, we develop a general linked-cluster formalism to calculate the single-particle and multi-particle contributions to the dynamical structure factor. We apply the method to the alternating Heisenberg chain (AHC), where expansions are done around the strong coupling limit of decoupled spin dimers up to 14th order in the ratio of coupling constants. We calculate various properties of the multiparticle continuum and bound states for a number of parameters including those appropriate for the material $Cu(NO_3)_2 \cdot 2.5D_2O$, which has recently been studied by neutron scattering [5,6].

The alternating Heisenberg chain is an excellent test-bed for our present purposes. It is a simple isotropic spin system with a finite energy gap (see Section III). The ground state is a spin singlet, and the lowest excitations are $S = 1$ triplet states. Above this band of 1-particle states there lies a 2-particle continuum. It was noted recently [7–9] that there are also 2-particle bound states with both $S = 0$ and $S = 1$ below the continuum, as well as quintuplet antibound states above it. Trebst et al. [1,10] found, in fact, that over a wide range of parameters there exist *two* singlet and *two* triplet bound states near the Brillouin zone boundary $kd = \pi$ (where d is the inter-dimer spacing). Hence the model displays some interesting multi-particle dynamics which can be explored both theoretically and experimentally. Neutron scattering experiments, however, will only be sensitive to the triplet bound states, which is what we focus on here.

There has been much discussion in the literature [11–13] about the behaviour of the alternating chain as it approaches the uniform limit, which is a critical point of the model. The uniform chain is gapless, and is known to exhibit

“spinon” excitations. The alternating chain is gapped, and is described in term of triplet excitations. The debate has concerned the behaviour of the model near the uniform limit, and how the transition is made from the “triplet” mode of description to the “spinon” mode. We discuss these questions further in Section IV.

We also directly obtain series expansions for sum-rules representing the total contributions of two-particle excitations to the dynamical structure factor summed over all wavevectors. Comparison of these with the static structure factor and the one-particle spectral weights, and extrapolations using approximant methods, leads to the conclusion that just keeping the one and two-particle excitations leads to a highly accurate description of the full dynamical structure factor, and this description remains quantitatively valid even in the uniform chain limit.

The plan of this paper is as follows. First, we discuss the formalism for calculating spectral weights using the linked cluster method. This is followed by detailed calculations of the spectral functions for the alternating Heisenberg chains. These are followed by our conclusions.

II. FORMALISM

We follow the formalism of Tennant et al. [6]. The inelastic neutron scattering cross-section [14]

$$\frac{d^2\sigma}{d\Omega d\omega} \propto N \sum_{\alpha,\beta} \frac{k_f}{k_i} |F(\mathbf{k})|^2 (\delta_{\alpha\beta} - k_\alpha k_\beta) S^{\alpha\beta}(\mathbf{k}, \omega) \quad (1)$$

is proportional to the “dynamical response” $S^{\alpha\beta}(\mathbf{k}, \omega)$ where \mathbf{k} is the wavevector transfer, $F(\mathbf{k})$ is the magnetic form factor, N is the number of scattering centres, k_i and k_f are the momenta of initial and final neutron states respectively, and $\alpha = x, y, z$ are Cartesian spin coordinates. The dynamical response is the space and time Fourier transform of the spin-spin correlation function

$$S^{\alpha\beta}(\mathbf{k}, \omega) = \frac{1}{2\pi N} \sum_{i,j} \int_{-\infty}^{\infty} \exp[i(\omega t + \mathbf{k} \cdot (\mathbf{r}_i - \mathbf{r}_j))] \langle S_j^\alpha(t) S_i^\beta(0) \rangle dt \quad (2)$$

where i and j label sites of the system. At temperature $T = 0$, the dynamical response becomes

$$S^{\alpha\beta}(\mathbf{k}, \omega) = \frac{1}{2\pi N} \sum_{i,j} \int_{-\infty}^{\infty} \exp[i(\omega t + \mathbf{k} \cdot (\mathbf{r}_i - \mathbf{r}_j))] \langle \psi_0 | S_j^\alpha(t) S_i^\beta(0) | \psi_0 \rangle dt \quad (3)$$

where $|\psi_0\rangle$ is the ground state of the Hamiltonian. This quantity is referred to as the neutron scattering “structure factor”. For the alternating Heisenberg chain, spin conservation and isotropy in spin space ensure that $S^{\alpha\beta} = 0$ for $\alpha \neq \beta$, and all diagonal spin components are equivalent,

$$S^{xx}(\mathbf{k}, \omega) = S^{yy}(\mathbf{k}, \omega) = S^{zz}(\mathbf{k}, \omega), \quad (4)$$

and

$$S^{xx}(\mathbf{k}, \omega) = \frac{1}{2} S^{-+}(\mathbf{k}, \omega). \quad (5)$$

Henceforth we concentrate our attention on $S^{-+}(\mathbf{k}, \omega)$.

A. Integrated Structure Factor

Integrating equation (2) over energy, we get:

$$\begin{aligned} S^{-+}(\mathbf{k}) &= \int_{-\infty}^{\infty} d\omega S^{-+}(\mathbf{k}, \omega) \\ &= \frac{1}{N} \sum_{i,j} \exp[i\mathbf{k} \cdot (\mathbf{r}_i - \mathbf{r}_j)] \langle S_j^- S_i^+ \rangle_0 \end{aligned} \quad (6)$$

which is just the Fourier transform of the spin-spin correlation function at $t = 0$. By translation invariance,

$$\langle S_j^- S_i^+ \rangle_0 = C^{-+}(i^*, \mathbf{r}_i - \mathbf{r}_j) \quad (7)$$

where i^* labels the position of i within the unit cell. In the present case, the unit cell consists of a single dimer. Therefore

$$S^{-+}(\mathbf{k}) = \sum_{\delta} C^{-+}(i^*, \delta) \exp[i\mathbf{k} \cdot \delta] \quad (8)$$

This quantity we shall refer to as the integrated structure factor.

B. Exclusive Structure Factors

Inserting a complete set of eigenstates $|\psi_\Lambda\rangle$ of H between the spin operators in equation (3), we can express the spin structure factor as a sum over “exclusive” structure factors

$$S^{-+}(\mathbf{k}, \omega) = \sum_{\Lambda} S_{\Lambda}^{-+}(\mathbf{k}, \omega) \quad (9)$$

where

$$S_{\Lambda}^{-+}(\mathbf{k}, \omega) = \frac{1}{2\pi N} \sum_{i,j} \int_{-\infty}^{\infty} dt \exp[i(\omega t + \mathbf{k} \cdot (\mathbf{r}_i - \mathbf{r}_j))] \langle \psi_0 | S_j^-(t) | \psi_{\Lambda} \rangle \langle \psi_{\Lambda} | S_i^+(0) | \psi_0 \rangle \quad (10)$$

Each exclusive structure factor $S_{\Lambda}^{-+}(\mathbf{k}, \omega)$ gives the intensity of scattering from $|\psi_0\rangle$ to a specific triplet excited state $|\psi_{\Lambda}\rangle$ [15]. In the Heisenberg picture $S_j^-(t) = \exp(iHt) S_j^-(0) \exp(-iHt)$ gives trivial exponentials in t , so the time integral simply gives an energy-conserving delta function

$$S_{\Lambda}^{-+}(\mathbf{k}, \omega) = \frac{1}{N} \delta(\omega - E_{\Lambda} + E_0) \left| \sum_i \langle \psi_{\Lambda} | S_i^+ | \psi_0 \rangle \exp[i\mathbf{k} \cdot \mathbf{r}_i] \right|^2 \quad (11)$$

Assuming the states $|\psi_{\Lambda}\rangle$ are eigenstates of momentum, the matrix elements of the spin operators at translationally equivalent sites are equal modulo a plane wave

$$\langle \psi_{\Lambda}(\mathbf{k}) | S_i^+ | \psi_0 \rangle = \langle \psi_{\Lambda}(\mathbf{k}) | S_{i^*}^+ | \psi_0 \rangle \exp[-i\mathbf{k} \cdot (\mathbf{r}_i - \mathbf{r}_{i^*})] \quad (12)$$

Then the sum over all sites i can be reduced to a sum over sites i^* in the unit cell

$$S_{\Lambda}^{-+}(\mathbf{k}, \omega) = \frac{N_c^2}{N} \delta(\omega - E_{\Lambda} + E_0) \left| \sum_{i^*} \langle \psi_{\Lambda}(\mathbf{k}) | S_{i^*}^+ | \psi_0 \rangle \exp[i\mathbf{k} \cdot \mathbf{r}_{i^*}] \right|^2 \quad (13)$$

where N_c is the number of unit cells on the lattice. It is convenient to define the “reduced exclusive structure factor” as

$$S_{\Lambda}^{-+}(\mathbf{k}, \omega) = N_c \delta(\omega - E_{\Lambda} + E_0) \left| \sum_{i^*} \langle \psi_{\Lambda}(\mathbf{k}) | S_{i^*}^+ | \psi_0 \rangle \exp[i\mathbf{k} \cdot \mathbf{r}_{i^*}] \right|^2 \quad (14)$$

If we sum over momenta, we obtain the autocorrelation function

$$\Phi(\omega) = \frac{1}{2\pi} \sum_{\mathbf{k}} S^{-+}(\mathbf{k}, \omega) \quad (15)$$

made up of exclusive contributions

$$\Phi_{\Lambda}(\omega) = \frac{1}{2\pi} \sum_{\mathbf{k}} S_{\Lambda}^{-+}(\mathbf{k}, \omega) \quad (16)$$

For the 2-particle continuum, one can also obtain the total auto-correlation function $\Phi_{\Lambda} = \sum_{\omega} \Phi_{\Lambda}(\omega)$.

We turn now to a discussion of algorithms for the calculation of exclusive structure factors within perturbation theory. Efficient linked cluster expansion methods have long been known [16–18,4] for calculating bulk properties of

a quantum lattice system. Similar methods for the calculation of 1-particle spectra were developed by Gelfand [19], and were extended to 2-particle spectra by Trebst et al [1,2].

Series methods for the calculations of exclusive 1-particle structure factors or spectral weights have been developed previously [20], and have been applied in several places (e.g. [21,9,22]). In this formalism, a cluster expansion was carried out directly for the structure factor itself. This formalism is inapplicable to the 2-particle bound states, however, because one needs to know the wavefunction of these states beforehand. Some leading order hand calculations for 2-particle states have recently been made [15,6]. The method proposed here performs a cluster expansion for the ‘exclusive matrix elements’, solving the effective 2-particle Hamiltonian to generate the required wavefunctions implicitly. A short paper giving some of our results has appeared recently [23]. We also note at this point that Knetter *et al.* [3] have used an alternative approach based on ‘continuous unitary transformations’ which is also capable of giving bound state energy spectra and structure factors to high order and in great detail, but this approach is more suitable to low dimension case.

Let us suppose that the Hamiltonian can be decomposed

$$H = H_0 + \lambda V \quad (17)$$

where H_0 is the unperturbed Hamiltonian and V is to be treated as a perturbation. We aim to expand the multiparticle dispersion relations and structure factors in powers of the parameter λ . For illustrative purposes, we shall use the language of the AHC, but the formalism can be applied more generally.

C. 1-particle states

At zeroth order, the ‘single-particle’ excitations in this model consist of triplet excitations on a single dimer which can be labelled $|\psi_\Lambda(m)\rangle$, where m is the position of the excited dimer, and Λ labels the angular momentum eigenstate (i.e. \mathbf{S}^2, S_z , in this case for AHC, the label Λ must correspond to the $(S, S_z) = (1, 1)$ state). In momentum space, the eigenstates will be

$$|\psi_\Lambda(k)\rangle = \frac{1}{\sqrt{N_c}} \sum_m \exp(i\mathbf{k} \cdot \mathbf{r}_m) |\psi_\Lambda(m)\rangle \quad (18)$$

This labelling can be retained at higher orders in perturbation theory as λ is raised from zero.

Then the matrix element

$$\langle \psi_\Lambda(k) | S_i^+ | \psi_0 \rangle = \frac{1}{\sqrt{N_c}} \sum_m \exp(-i\mathbf{k} \cdot \mathbf{r}_m) \langle \psi_\Lambda(m) | S_i^+ | \psi_0 \rangle \quad (19)$$

It follows from translation invariance that the matrix element $\langle \psi_\Lambda(m) | S_i^+ | \psi_0 \rangle$ in this expression is a function of $(\mathbf{r}_i - \mathbf{r}_m)$ only, i.e., we can define the exclusive matrix elements

$$\Omega_\Lambda^{1p}(i^*, \boldsymbol{\delta}) \equiv \langle \psi_\Lambda(m) | S_i^+ | \psi_0 \rangle \quad (20)$$

where $\boldsymbol{\delta}$ is the distance between i and m , $\boldsymbol{\delta} = \mathbf{r}_i - \mathbf{r}_m$, and i^* labels site i within the unit cell as before.

The reduced exclusive structure factor is

$$S_\Lambda^{-+}(\mathbf{k}) = \left| \sum_{i^*, \boldsymbol{\delta}} \Omega_\Lambda(i^*, \boldsymbol{\delta}) \exp[i\mathbf{k} \cdot \boldsymbol{\delta}] \right|^2 \quad (21)$$

D. 2-particle states

Since two triplets can combine to give total spin 1, there will also be non-zero spin structure factors for 2-particle states. The 2-particle states can be labelled according to their unperturbed counterparts in position space $|\psi_\Lambda(m, n)\rangle$ where m, n label the two dimer positions, and Λ the corresponding total 2-particle angular momentum states. Eigenstates of the Hamiltonian can then be expanded

$$|\psi_\Lambda(\mathbf{k})\rangle = \frac{1}{\sqrt{N_c}} \sum_{m, n} f_\Lambda(\mathbf{r}_m - \mathbf{r}_n) e^{i\mathbf{k} \cdot (\mathbf{r}_m + \mathbf{r}_n)/2} |\psi_\Lambda(m, n)\rangle \quad (22)$$

where $f_\Lambda(\mathbf{r}_m - \mathbf{r}_n)$ is the 2-particle wavefunction, which only depends on the relative distance $\mathbf{r}_m - \mathbf{r}_n$.

Similarly one can define the 2-particle exclusive matrix elements

$$\Omega_\Lambda^{2p}(i; m, n) \equiv \langle \psi_\Lambda(m, n) | S_i^+ | \psi_0 \rangle \quad (23)$$

The translation invariance implies that $\Omega_\Lambda^{2p}(i; m, n)$ only depends on the relative distance between m, n and i , i.e.

$$\Omega_\Lambda^{2p}(i; m, n) \equiv \Omega_\Lambda^{2p}(i^*, \mathbf{r}, \boldsymbol{\delta}) \quad (24)$$

where $\mathbf{r} = (2\mathbf{r}_i - \mathbf{r}_m - \mathbf{r}_n)/2$ and $\boldsymbol{\delta} = \mathbf{r}_m - \mathbf{r}_n$.

Then, we can get the reduced 2-particle exclusive structure factor as

$$S_\Lambda^{-+}(\mathbf{k}, \omega) = \delta(\omega - E_\Lambda + E_0) \left| \sum_{i^*, \mathbf{r}, \boldsymbol{\delta}} \Omega_\Lambda^{2p}(i^*, \mathbf{r}, \boldsymbol{\delta}) f_\Lambda(\boldsymbol{\delta}) \exp[i\mathbf{k} \cdot \mathbf{r}] \right|^2 \quad (25)$$

E. Cluster expansion

It is easy to see that the exclusive matrix elements $\Omega_\Lambda^{1p}(\boldsymbol{\delta})$ and $\Omega_\Lambda^{2p}(\mathbf{r}, \boldsymbol{\delta})$ obey a simple ‘cluster addition’ property. If a cluster C is made up of two disconnected sub-clusters A and B, then¹

$$\Omega_\Lambda^{1p,C}(\boldsymbol{\delta}) = \Omega_\Lambda^{1p,A}(\boldsymbol{\delta}) + \Omega_\Lambda^{1p,B}(\boldsymbol{\delta}) \quad (26)$$

$$\Omega_\Lambda^{2p,C}(\mathbf{r}, \boldsymbol{\delta}) = \Omega_\Lambda^{2p,A}(\mathbf{r}, \boldsymbol{\delta}) + \Omega_\Lambda^{2p,B}(\mathbf{r}, \boldsymbol{\delta}) \quad (27)$$

where $\Omega_\Lambda^{1p,A}(\boldsymbol{\delta})$ is trivially *zero* if cluster A does not contain both dimer m and site i , by conservation of spin, and similarly for $\Omega_\Lambda^{2p,A}(\mathbf{r}, \boldsymbol{\delta})$. It follows that the elements Ω_Λ admit a linked cluster expansion

$$\Omega_\Lambda = \sum_{\gamma} \Omega_\Lambda^\gamma \quad (28)$$

where the sum over γ denotes a sum over all connected clusters. Correspondingly, the perturbation series expansion for Ω_Λ could be formulated in terms of a diagrammatic expansion where only connected diagrams contribute, although we will not elaborate on this approach here.

An efficient linked cluster algorithm for calculation of the structure factors can now be formulated, following Trebst et al. [1,2]:

- i) Generate a list of connected clusters γ appropriate to the problem at hand (in the present case, they will simply consist of chains of dimers of different lengths);
- ii) For each cluster γ , construct matrices for the Hamiltonian H and spin operators S_i^+ in the basis of singlet and triplet dimer states corresponding to H_0 ;
- iii) ‘Block diagonalize’ the Hamiltonian by an orthogonal transformation

$$H^{\text{eff}} = O^T H O \quad (29)$$

as outlined by Trebst et al [1,2], constructed order-by-order in perturbation theory so that the 1-particle states sit in a block by themselves, and similarly the 2-particle states, etc; with this one can compute the exclusive matrix elements Ω_Λ .

- iv) Subtract all sub-cluster contributions to get the cumulant $\Omega_\Lambda(\boldsymbol{\delta})$;

¹We suppress the starred cell index i^* , henceforth.

- v) Insert the cumulant $\Omega_\Lambda(\delta)$ in Eq. (28), and hence one can build up the exclusive matrix elements for the bulk system.
- vi) For the 1-particle case, one can insert the exclusive matrix elements into Eq. (21) to get the series for the exclusive structure factors. For the 2-particle case, one still needs to solve the effective 2-particle Hamiltonian to get the wavefunctions f_Λ for the possible bound states and continuum: this can be done by using the finite lattice approach [2]. To get the series solution rather than the numerical solution for the wavefunctions f_Λ and the 2-particle dispersion relation, one has to use degenerate perturbation theory. With the results for exclusive matrix elements Ω_Λ and wavefunctions f_Λ in hand, one can get the exclusive structure factor S_Λ through Eq. (25).

III. RESULTS FOR THE ALTERNATING HEISENBERG CHAIN

We apply this method to investigate the spectral weights of the alternating Heisenberg chain, which can be described by the following Hamiltonian

$$H = \sum_i \mathbf{S}_{2i} \cdot \mathbf{S}_{2i+1} + \lambda \mathbf{S}_{2i-1} \cdot \mathbf{S}_{2i} \quad (30)$$

where the \mathbf{S}_i are spin- $\frac{1}{2}$ operators at site i , and λ is the alternating coupling. Here we assume that the distance between neighboring spins are all equal and the distance between two successive dimers is d , and assume $d = 1$ if it does not appear explicitly (note this is different from our previous paper [10], where we had taken the lattice spacing a to be 1).

There is a considerable literature on this model, which has been reviewed recently by Barnes et al. [15]. At $\lambda = 0$, the system consists of a chain of decoupled dimers, and in the ground state each dimer is in a singlet state. Excited states are made up from the three triplet excited states on each dimer, with a finite energy gap between the singlet ground state and the triplet excited states. This scenario is believed [24–26] to hold right up to the uniform limit $\lambda = 1$, which corresponds to a critical point. At $\lambda = 1$, we regain the uniform Heisenberg chain, which is gapless.

Several theoretical papers [11–13] have discussed the approach to the uniform limit. Analytic studies of the critical behaviour near $\lambda = 1$ [11] have related the alternating chain to the 4-state Potts model, and indicate that the ground-state energy per site $\epsilon_0(\lambda)$, and the energy gap $\Delta(\lambda)$ should behave as

$$\begin{aligned} \epsilon_0(\lambda) - \epsilon_0(1) &\sim \delta^{4/3} / |\ln(\delta/\delta_0)| \\ \Delta(\lambda) &\sim \delta^{2/3} / \sqrt{|\ln(\delta/\delta_0)|} \end{aligned} \quad (31)$$

as $\lambda \rightarrow 1$, where $\delta = (1 - \lambda)/(1 + \lambda)$. The logarithmic terms are due to the existence of a marginal variable in the model.

Numerical studies of the model include series expansions [24,25,22], and exact diagonalizations for finite lattices [27,28]. Recently, Papenbrock *et al.* [29] have carried out density-matrix renormalization group studies on lattices up to 192 sites in extent. They conclude that the data for the ground-state energy and triplet energy gap are consistent with Eq. (31), but with surprisingly large scale factors δ_0 in the logarithms. Dlog Padé analysis of the series supports these conclusions [22].

The 2-triplet bound states were previously studied by Uhrig and Schulz [7] using an RPA approach. They found a singlet bound state below the 2-particle continuum for all momenta k and over the whole range of $1 > \lambda > 0$. They also predicted a triplet bound state and a quintuplet antibound state near $kd = \pi$ for small λ . These conclusions were supported in later studies [8,9,30]. Barnes et al. [15] and Tennant et al. [6] have shown how to calculate exclusive structure factors for the 2-particle states by low-order series expansions in λ , and have made a comparison with experimental data for the copper nitrate material, $\text{Cu}(\text{NO}_3)_2 \cdot 2.5\text{D}_2\text{O}$. They find that the experimental data are consistent with the existence of a bound state, but do not yet constitute definitive proof of it. They highlight the need for more powerful perturbative techniques to calculate these multiparticle cross sections: the present paper is aimed at meeting this need [23].

We have recently made an extensive study of the two triplet bound states of this model using high-order series expansions [1,10]. We found that in fact there are *two* singlet (S_1 and S_2) and *two* triplet (T_1 and T_2) bound states below the two-particle continuum, and *two* quintet antibound states (Q_1 and Q_2) above the continuum, for λ not too

large. Meanwhile, Schmidt and Uhrig [31] have used a different technique, the ‘continuous unitary transformations’ (CUTS) method, to study the model at high orders in perturbation theory. We shall compare our results with theirs in what follows.

Here we study the structure factors using series expansions. We have computed, up to order λ^{13} , the series for the integrated structure factor $S(k)$ and the exclusive structure factors for the 1-particle triplet state $S_{1p}(k)$. For the 2-particle states, we also computed the total 2-particle structure factor S_{2p} (summed over all 2-particle states) up to order λ^{13} , and to order λ^{12} for the exclusive matrix elements $\Omega_{\Lambda}^{2p}(r, \delta)$. With these we can compute the structure factors for the 2-particle triplet bound states (i.e. S_{T_1} for T_1 and S_{T_2} for T_2), and for the 2-particle continuum S_{2pc} up to order λ^{14} . Integrating the structure factor over momentum k , we can also compute the series for the auto-correlation function defined in Eq. (15). We have computed the auto-correlation functions for the 1-particle (Φ_{1p}), and 2-particle sectors (Φ_{2p}), and the individual auto-correlation functions for 2-particle bound states T_1 (Φ_{T_1}) and T_2 (Φ_{T_2}) and the 2-particle continuum (Φ_{2pc}). Full series for $S(k)$ and $S_{1p}(k)$ are given in Tables I and II. Some other selective series (at $kd \rightarrow 0$, $kd = \pi$, and 2π) are given in Table III, other series are available on request.

The 1-particle structure factor has been computed to order λ^3 by Barnes *et al.* [15], but our series disagree with their results from second order. In their calculation, they neglect the first term in their Eq. (56); they claim this term is zero due to a symmetry relation, but actually this only holds in leading order. Recently Müller and Mikeska [32] have extended the series for the 1-particle structure factor $S_{1p}(k)$ to order λ^{10} , and our series agree with theirs. The auto-correlation functions for 1-particle (Φ_{1p}) and 2-particle (Φ_{2p}) states have been recently computed up to order λ^7 by Schmidt and Uhrig [31], and our results also agree with theirs, but extend the series by up to 6 terms. As a byproduct of our calculation, we have computed the series for 1-triplet excitation spectra up to order λ^{13} , and the series for 2-triplet excitation spectra up to order λ^{12} , this extends the previous calculations [10] by two terms for 1-triplet excitation spectra, and by 1 term for 2-triplet excitation spectra. These series are available on request. We use Dlog Padé approximants and integrated differential approximants [33] to obtain numerical results up to $\lambda = 1$.

A. The integrated structure factor S

The integrated structure factor² S has been computed up to order λ^{13} . It can be expressed as

$$S(kd) = 1 - \cos(kd/2) + \sum_{m=1}^{\infty} \sum_{n=1}^{2m+1} a_{n,m} \lambda^m \cos(nkd/2) \quad (32)$$

The series coefficients $a_{n,m}$ are given in Table I. Note that there are two general relations for these coefficients:

$$\sum_{n=1}^{2m+1} a_{n,m} = 0 \quad (33)$$

$$a_{2m,m} = -2a_{2m+1,m}$$

With this, one can easily prove that $S(k)$ can be written in the following form with a common factor $\sin^2(kd/4)$ at all orders

$$S(kd) = \sin^2(kd/4) \sum_{m=0}^{\infty} \sum_{n=0}^{2m} b_{n,m} \lambda^m \cos(nkd/2) \quad (34)$$

where one of the coefficients $b_{2m-1,m}$ happens to be zero always for any m , due to the second relation in Eq. (33). For example, the series up to order λ^4 can be written as

$$S(kd) = \sin^2\left(\frac{kd}{4}\right) \left[2 + \lambda \cos(kd) + \frac{\lambda^2}{8} \left(2 + 4 \cos\left(\frac{kd}{2}\right) + 3 \cos(kd) + 3 \cos(2kd) \right) \right]$$

²We drop the superscripts $-+$ henceforth.

$$\begin{aligned}
& + \frac{\lambda^3}{96} \left(12 + 24 \cos\left(\frac{kd}{2}\right) + 13 \cos(kd) + 16 \cos\left(\frac{3kd}{2}\right) + 28 \cos(2kd) + 15 \cos(3kd) \right) \\
& + \frac{\lambda^4}{4608} \left(346 + 692 \cos\left(\frac{kd}{2}\right) + 669 \cos(kd) + 912 \cos\left(\frac{3kd}{2}\right) + 784 \cos(2kd) + 304 \cos\left(\frac{5kd}{2}\right) \right. \\
& \left. + 852 \cos(3kd) + 315 \cos(4kd) \right) + O(\lambda^5) \Big] \tag{35}
\end{aligned}$$

To analyze the series $S(kd)$, we firstly consider $S(kd)$ near two special momentum points, $kd = 0$ and $kd = 2\pi$. We know that $S = 0$ at $k = 0$, but it is interesting to study how it vanishes as $k \rightarrow 0$. For small λ , it is trivial to see from Eq.(35) that $S \propto k^2$ as $k \rightarrow 0$. Thus we can define $R = \lim_{kd \rightarrow 0} S(kd)/(kd)^2$, and the series for R is given in Table III. Applying Dlog Padé approximants to this series, we find that R diverges at $\lambda = 1$, with a critical index about -0.71^3 . This implies that for the uniform chain, $\lambda = 1$, $S(kd)$ no longer vanishes quadratically with k . Naively one might then expect it to vanish linearly as $k \rightarrow 0$: some evidence for this is shown in Fig. 1.

For the uniform chain $\lambda = 1$, and near $kd \rightarrow 2\pi$, Affleck has argued [34] the asymptotic form for $S(kd)$ as

$$S(kd) = \frac{8}{3(2\pi)^{3/2}} |\ln(\pi - kd/2)|^{3/2} \tag{36}$$

This implies that for $kd = 2\pi$ and as $\lambda \rightarrow 1$, the asymptotic form for $S(2\pi)$ diverges as

$$S(2\pi) \propto [-\ln(1 - \lambda)]^{3/2} \quad \lambda \rightarrow 1 \tag{37}$$

If so, one should be able to see a critical point at $\lambda = 1$ with critical index -1 if one applies Dlog Padé approximants [33] to the series $\partial S^{2/3}/\partial \lambda$. This is indeed the case as we can see from Table IV. Note, however, that very similar results are obtained for any index between $3/2$ and 1 , so this is not a very sensitive test.

Assuming the above asymptotic form for $S(2\pi)$ is correct, we can also estimate the prefactor of this asymptotic form by using integrated different approximants [33] to extrapolate the series for $S(2\pi)/[1 - \ln(1 - \lambda)]^{3/2}$ to $\lambda = 1$. The result is:

$$S(2\pi) = 0.19(2) [-\ln(1 - \lambda)]^{3/2} \quad \lambda \rightarrow 1 \tag{38}$$

The prefactor agrees with Affleck's prediction of $8/3(2\pi)^{3/2} = 0.16932$.

For $0 < kd < 2\pi$, one expects S to be finite for any λ . The results for S versus momentum k for $\lambda = 0, 0.6$, and 1 are shown in Fig. 1. Note that $\int_0^{2\pi} S(k) dk = 2\pi$ (here we set $d = 1$), independent of λ , so the area under each curve is the same. Also shown in the figure are the results for $S' \equiv 6S[-2\pi \ln(1 - \frac{k}{2\pi})/k]^{-3/2}$ at $\lambda = 1$.

For fixed values of k , Fig. 2 shows the integrated structure factor S versus λ , where for each value of k , about 20 different integrated differential approximants to the series are shown. We can see that the results converge very well out to $\lambda = 1$. The logarithmic divergence as $\lambda \rightarrow 1$ for the case $kd = 2\pi$ is clearly evident.

B. The 1-particle spectral weight

The exclusive 1-particle structure factor $S_{1p}(kd)$ has been computed up to order λ^{13} . S_{1p} can also be expressed as

$$S_{1p}(kd) = \sum_{n,m} a_{n,m} \lambda^m \cos(nkd/2) \tag{39}$$

The series coefficients $a_{n,m}$ are given in Table II. The coefficients $a_{n,m}$ also satisfy Eq. (33), and $S_{1p}(kd)$ also has a common factor $\sin^2(kd/4)$ for all orders. The series up to order λ^4 can be written as

$$\begin{aligned}
S_{1p}(kd) = \sin^2\left(\frac{kd}{4}\right) & \left[2 + \lambda \cos(kd) + \frac{\lambda^2}{8} \left(-1 + 8 \cos\left(\frac{kd}{2}\right) + 2 \cos(kd) + 3 \cos(2kd) \right) \right. \\
& \left. + \frac{\lambda^3}{96} \left(36 \cos\left(\frac{kd}{2}\right) + 17 \cos(kd) + 8 \cos\left(\frac{3kd}{2}\right) + 32 \cos(2kd) + 15 \cos(3kd) \right) \right]
\end{aligned}$$

³Within the accuracy of our calculations this is consistent with a value of $2/3$ with logarithmic corrections

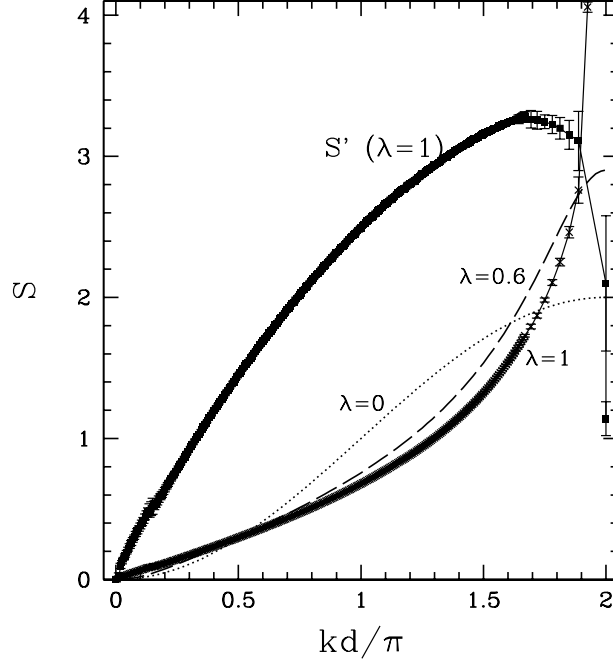


FIG. 1. The integrated structure factor S versus k for $\lambda = 0$ (dotted line), 0.6 (dashed line), 1 (crosses). Also shown is the quantity $S' \equiv 6S[-2\pi \ln(1 - \frac{k}{2\pi})/k]^{-3/2}$ for $\lambda = 1$ (squares).

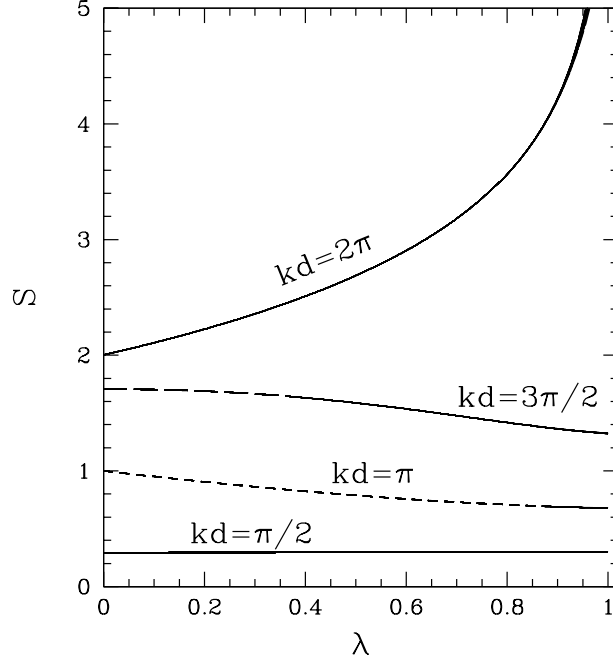


FIG. 2. The integrated structure factor S versus λ for $kd = \pi/2, \pi, 3\pi/2$ and 2π . For each value of kd , about 20 different integrated differential approximants to the high-temperature series are shown, though most of them are indistinguishable on the scale of this figure.

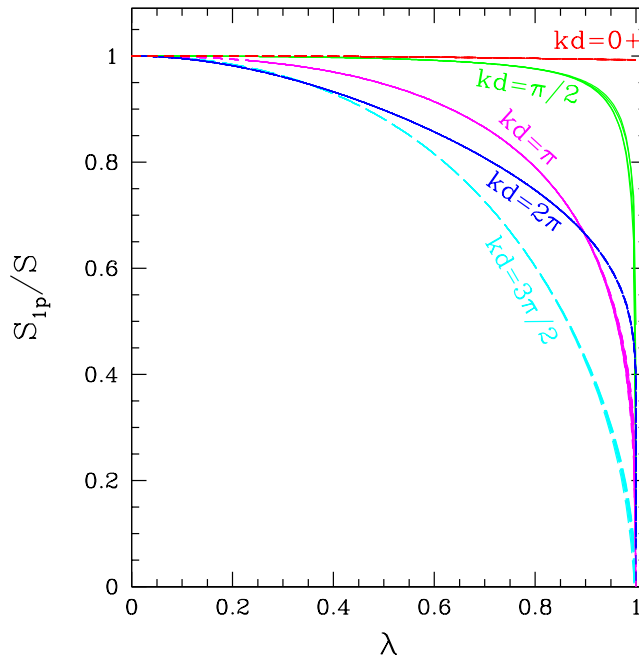


FIG. 3. The relative 1-particle weight S_{1p}/S versus λ for $kd = 0+, \pi/2, \pi, 3\pi/2$ and 2π . Several different integrated differential approximants to the series are shown.

$$\begin{aligned}
& + \frac{\lambda^4}{4608} \left(342 + 384 \cos\left(\frac{kd}{2}\right) + 784 \cos(kd) + 856 \cos\left(\frac{3kd}{2}\right) + 675 \cos(2kd) + 368 \cos\left(\frac{5kd}{2}\right) \right. \\
& \left. + 804 \cos(3kd) + 315 \cos(4kd) \right) + O(\lambda^5) \Big] \quad (40)
\end{aligned}$$

Let us analyze the behaviour of S_{1p} when $\lambda \rightarrow 1$. For $kd = 2\pi$, our analysis shows that S_{1p} is finite as $\lambda \rightarrow 1$, so S_{1p}/S vanishes like $1/[-\ln(1-\lambda)]^{3/2}$. For the case $kd = 0$, we again define $R_{1p} \equiv \lim_{kd \rightarrow 0} S_{1p}(kd)/(kd)^2$ (note that R_{1p} differs from R from order λ^4). The Dlog Padé approximants to R_{1p} show that it diverges at $\lambda = 1$ with critical index about -0.71. This again implies that for the uniform chain case ($\lambda = 1$), S_{1p} no longer vanishes as k^2 . Now let us analyze the series for the relative spectral weight R_{1p}/R . The Dlog Padé approximants to the series R_{1p}/R show no singularity near $\lambda = 1$. This means that as $\lambda \rightarrow 1$, R_{1p}/R remains finite. Our extrapolations show $R_{1p}/R = 0.993(1)$ at $\lambda = 1$.

For $0 < kd < 2\pi$, the analysis of the series S_{1p} by the Dlog Padé approximants shows that it vanishes with a behavior close to $(1-\lambda)^{1/3}$. Since S remains finite, we thus expect that S_{1p}/S vanishes like $(1-\lambda)^{1/3}$. This agrees with the analysis of Schmidt and Uhrig [31], who argued that the 1-particle spectral weight should vanish like $\sqrt{\Delta}$, i.e. like $\delta^{1/3}/|\ln(\delta/\delta_0)|^{1/4}$, where $\delta = (1-\lambda)/(1+\lambda)$. Fig. 3 shows the relative 1-particle weight S_{1p}/S versus λ at selected values of kd . It can be seen that for any non-zero value of k , S_{1p}/S decreases abruptly to zero as $\lambda \rightarrow 1$. Only at $kd = 0+$, does S_{1p}/S remain finite (about 0.993) in the limit $\lambda = 1$; but by then S has itself decreased to zero.

The overall picture that emerges is that as $\lambda \rightarrow 1$ the triplet energy gap goes to zero, and the spectral weight associated with the 1-triplet state also vanishes [22]. This would seem to agree with the idea that the “spinons”, rather than the triplet states, act as the elementary excitations in the model in the uniform limit $\lambda \rightarrow 1$.

Fig. 4 shows the relative 1-particle weight S_{1p}/S versus k for $\lambda = 0.27, 0.5, 0.7, 0.8, 0.90367$, where $\lambda = 0.90367$ is the estimated coupling for CuGeO_3 [7]. For $\lambda = 0.90367$, we can see that S_{1p}/S is about 1 for small k , and has a minimum around $kd = 1.6\pi$ with value 0.43, whereas Uhrig and Schulz [7] estimated $S_{1p}/S = 0.28$.

C. The 2-particle spectral weight

As we mentioned before, there are two triplet bound states (T_1 and T_2) in this system. Before we discuss the spectral weight for individual states, let us first discuss the total spectral weight (the sum rule) for all 2-particle

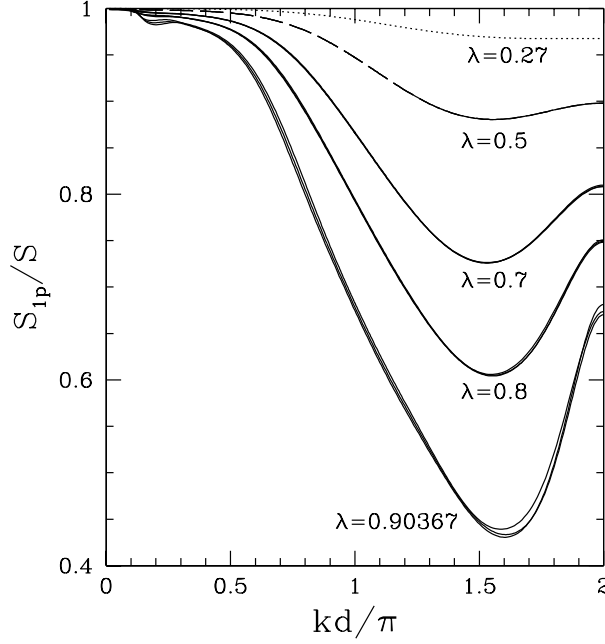


FIG. 4. The relative 1-particle weight S_{1p}/S versus k for $\lambda = 0.27, 0.5, 0.7, 0.8, 0.90367$. The results of the three highest orders are plotted.

states.

1. The total 2-particle spectral weight

The total 2-particle structure factor (S_{2p}) has been computed up to order λ^{12} . This quantity $S_{2p}(kd)$ also has a common factor $\sin^2(kd/4)$ for all orders, and the series up to order λ^4 can be written as

$$S_{2p}(kd) = \sin^2\left(\frac{kd}{4}\right) \left[\lambda^2 \sin^4\left(\frac{kd}{4}\right) + \frac{\lambda^3}{12} \left(3 + 2 \cos\left(\frac{3kd}{2}\right) \right) \sin^2\left(\frac{kd}{4}\right) + \frac{\lambda^4}{4608} \left(-57 + 372 \cos\left(\frac{kd}{2}\right) - 143 \cos(kd) \right) \right. \\ \left. + 64 \cos\left(\frac{3kd}{2}\right) + 108 \cos(2kd) - 64 \cos\left(\frac{5kd}{2}\right) + 48 \cos(3kd) \right] + O(\lambda^5) \quad (41)$$

Here $S_{2p} \propto k^2$ in the limit $k \rightarrow 0$, and so we again define $R_{2p} \equiv \lim_{k \rightarrow 0} S_{2p}(kd)/(kd)^2$. Note that R_{2p} is nonzero from order λ^4 , while S_{2p} with $k \neq 0$ is nonzero from order λ^2 .

Fig. 5 shows the total 2-particle weight S_{2p}/S versus k for various λ . For large λ , S_{2p}/S has a maximum around $kd = 1.6\pi$. For $\lambda = 0.6$, it has a value of about 0.1848 at its maximum, while the value for $k = 0$ is only 0.00177, about 100 times smaller than the maximum.

For fixed values of k , Fig. 6 shows the relative total 2-particle weight S_{2p}/S versus λ for $kd = \pi/2, \pi, 3\pi/2$ and 2π . We can see that there are some sharp increases near $\lambda = 1$ which make it difficult to estimate the results; nevertheless, we estimate, at $\lambda = 1$, the 2-particle states have about 90% of the total weight at $kd = 3\pi/2$, about 80% of the weight at $kd = 2\pi$, about 65% of the weight at $kd = \pi$, and only about 10% of the weight at $kd = \pi/2$. We also show the results for $15S_{2p}/(\lambda^2 S)$ in the special case $k = 0$, which show quite different behaviour from other k in this figure: as λ increases, it increases firstly, then decreases, so that the relative weight at $\lambda = 1$ is tiny (less than 0.5%). This agrees with the fact that the relative weight for the 1-particle state, R_{1p}/R , is almost 99.27% at $\lambda = 1$ for this value of k .

Subtracting the weight of 1 and 2-particle states from the total weight, one can obtain the remaining weight $(S - S_{1p} - S_{2p})/S$ for states of more than two-particles. The results for various λ are shown in Fig. 7. For small λ , the remaining weight increases as k increases, while for larger λ , it develops a peak near $kd = 1.5\pi$, and the remaining weight near $kd = 2\pi$ decreases as λ increases. These weights are tiny, as can be seen, but increasing with λ .

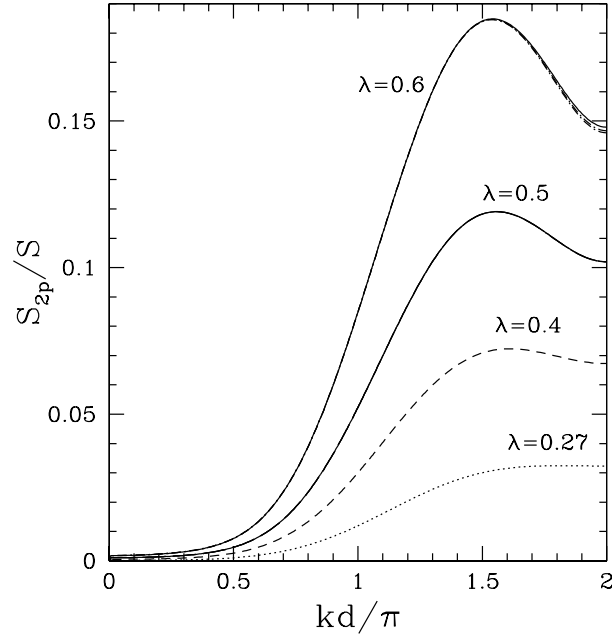


FIG. 5. The relative 2-particle weight S_{2p}/S versus k for $\lambda = 0.27, 0.4, 0.5, 0.6$. The results of the three highest orders are plotted.

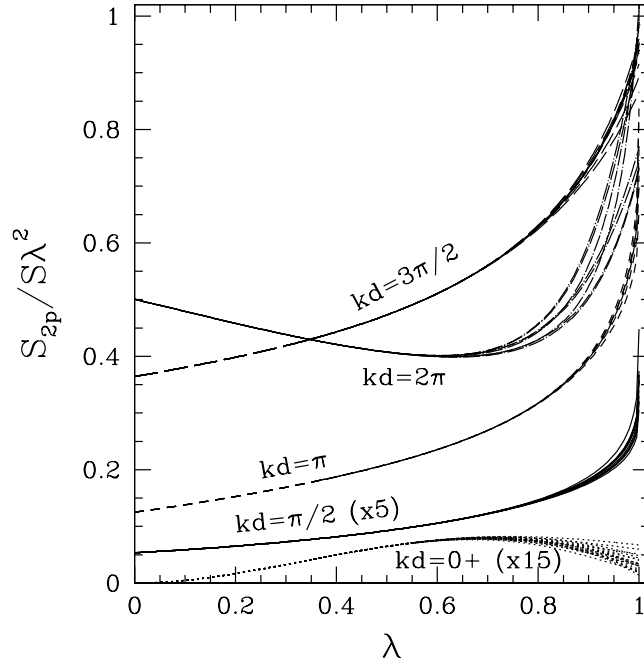


FIG. 6. The relative 2-particle weight S_{2p}/S versus λ for $kd = 0+, \pi/2, \pi, 3\pi/2$ and 2π . The results for $kd = 0+ (\pi/2)$ are multiplied by a factor 15 (5) to make them more visible on the graph. Several different integrated differential approximants to the series are shown.

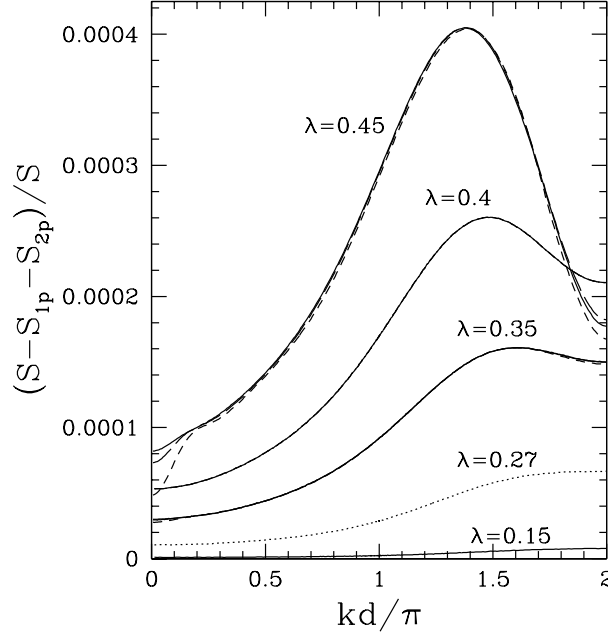


FIG. 7. The remaining spectral weight for states of more than 2-particles $((S - S_{1p} - S_{2p})/S)$ for $\lambda = 0.15, 0.27, 0.35, 0.4, 0.45$. The results of the three highest orders are plotted.

2. The individual weights for triplet bound states and continuum

For the bound state T_1 , we can obtain an analytic expression for its structure factor up to order λ^3

$$S_{T_1}(kd) = -\lambda^2 (1 + 2 \cos(kd)) \sin^6\left(\frac{kd}{4}\right) - \frac{\lambda^3}{24} \left(-60 + 101 \cos\left(\frac{kd}{2}\right) - 102 \cos(kd) \right. \\ \left. + 69 \cos\left(\frac{3kd}{2}\right) - 48 \cos(2kd) + 22 \cos\left(\frac{5kd}{2}\right) \right) \sin^4\left(\frac{kd}{4}\right) + O(\lambda^4) \quad (42)$$

where the λ^2 term agrees with that obtained by Barnes *et al.* [6]

As a byproduct of our calculations, we also get an analytic expression for the coherence length [2] which is defined as

$$L = \frac{\sum_{\mathbf{r}} |\mathbf{r}| f_{\mathbf{r}}^2}{\sum_{\mathbf{r}} f_{\mathbf{r}}^2} \quad (43)$$

where $f_{\mathbf{r}}$ is the amplitude (the eigenvector) for two single-particle excitations separated by distance \mathbf{r} (see Eq. 22). The result up to order λ^2 for bound state T_1 is

$$\frac{1}{L_{T_1}} = -1 - 2 \cos(kd) + \frac{\lambda}{2} [-24 - 36 \cos(kd) - 17 \cos(2kd) - 5 \cos(3kd)] + \frac{\lambda^2}{32} \left[-3410 \right. \\ \left. - 5937 \cos(kd) - 3768 \cos(2kd) - 1619 \cos(3kd) - 482 \cos(4kd) - 100 \cos(5kd) \right] + O(\lambda^3) \quad (44)$$

With these expressions, one can determine the critical momentum k_c where S_{T_1} or $1/L_{T_1}$ vanishes. For both S_{T_1} or $1/L_{T_1}$, one gets the same k_c as

$$k_c d = \begin{cases} 2\pi/3 + 5\lambda/(4\sqrt{3}) - 757\lambda^2/(192\sqrt{3}) + O(\lambda^3), & k_c d < \pi \\ 4\pi/3 - 5\lambda/(4\sqrt{3}) + 757\lambda^2/(192\sqrt{3}) + O(\lambda^3), & k_c d > \pi \end{cases} \quad (45)$$

This agrees with previous results obtained from the two-particle binding energy [10]. The expressions (42) and (44) are valid within these regions of momentum. In the limit $k \rightarrow k_c$, the behaviours of $S_{T_1}(k)$ or $1/L_{T_1}$ are

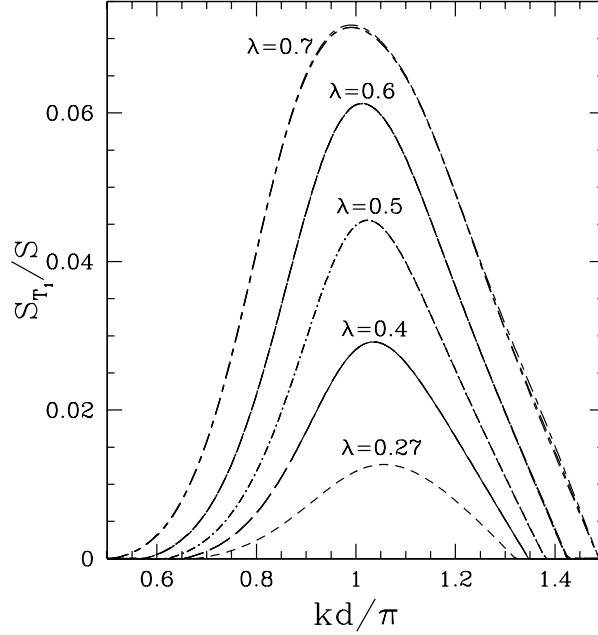


FIG. 8. The relative weight for bound state T_1 (S_{T_1}/S) for $\lambda = 0.27, 0.4, 0.5, 0.6, 0.7$. The results of the three highest orders are plotted.

$$S_{T_1}(k) = \begin{cases} (k - k_c)d \lambda^2 (24 + 29\lambda)/(512\sqrt{3}) + O(\lambda^4), & k_c d < \pi \\ 9\sqrt{3}(k_c - k)d (24 - 31\lambda) \lambda^2/512 + O(\lambda^4), & k_c d > \pi \end{cases} \quad (46)$$

$$1/L_{T_1} = \frac{|k - k_c|d (144 + 12\lambda - 443\lambda^2)}{48\sqrt{3}} \quad (47)$$

So as $k \rightarrow k_c$, $S_{T_1}(k)$ and $1/L_{T_1}$ are proportional to $(k - k_c)$, whereas the binding energy is proportional to $(k - k_c)^2$ [10].

Integrating S_{T_1} in Eq. (42) over the momenta given in Eq. (45), one can get the auto-correlation function for T_1 as

$$\Phi_{T_1} = \lambda^2 \left(-\left(\frac{1}{6}\right) + \frac{23\sqrt{3}}{64\pi} \right) + \lambda^3 \left(\frac{433}{576} - \frac{361\sqrt{3}}{256\pi} \right) + O(\lambda^4) \quad (48)$$

Since the bound state T_2 only appears at $kd = \pi$ in the small λ limit, we cannot get a similar analytic expression for it, nor for the 2-particle continuum. But the series for exclusive 2-particle matrix elements Ω_Λ^{2p} have been computed up to order λ^{12} , and with this one can compute numerical results, for any given value of k , for the exclusive structure factor of the 2-particle triplet bound states (T_1 and T_2) and 2-particle continuum through the finite lattice approach [10]. We can also get some series in λ for the structure factor over those momenta k where the bound states appear in the limit $\lambda \rightarrow 0$, and the series for $kd = \pi$ are given in Table III.

The relative spectral weights for T_1 and T_2 versus k are shown in Figs. 8 and 9 for several values of λ . The weight for T_1 is nonzero only over a finite range of momentum where the bound state exists. In the limit $\lambda \rightarrow 0$, S_{T_1}/S has a maximum at $kd = 4 \arccos(\sqrt{(5 - \sqrt{3})/8}) = 1.117\pi$, and as λ increases, the maximum position $k_0 d$ moves towards to $k_0 d = \pi$. The results for $k_0 d$ as function of λ are given in Fig. 10. The relative spectral weight for T_2 exhibits an interference zero near $kd \sim \pi$, which can be traced back to the bound-state wave function for $\lambda \rightarrow 0$, where the two triplets are separated by an odd number of dimers [10]. The position of this zero shifts to smaller k as λ increases, and is also shown in Fig. 10. Another interesting feature here is that the spectral weight vanishes like $(k - k_c)^2$ as $k \rightarrow k_c$, rather than $(k - k_c)$ as we have seen in Eq. (46). Also shown in Fig. 10 is the location of the maximum relative weight for T_2 .

The remaining weight for the 2-particle continuum S_{2pc} is shown in Fig. 11. These curves show a dip near $kd = \pi$, because the bound states absorb some of the weight in that region.

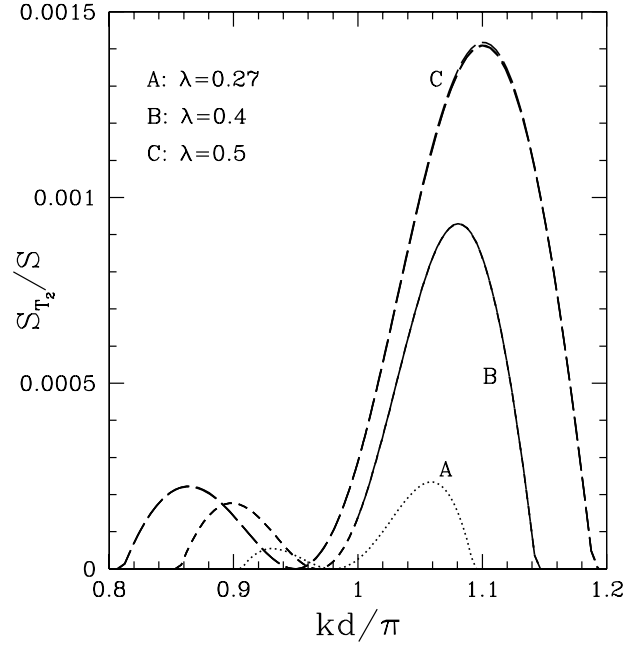


FIG. 9. The relative weight for bound state T_2 (S_{T_2}/S) for $\lambda = 0.27, 0.4, 0.5$. The results of the three highest orders are plotted.

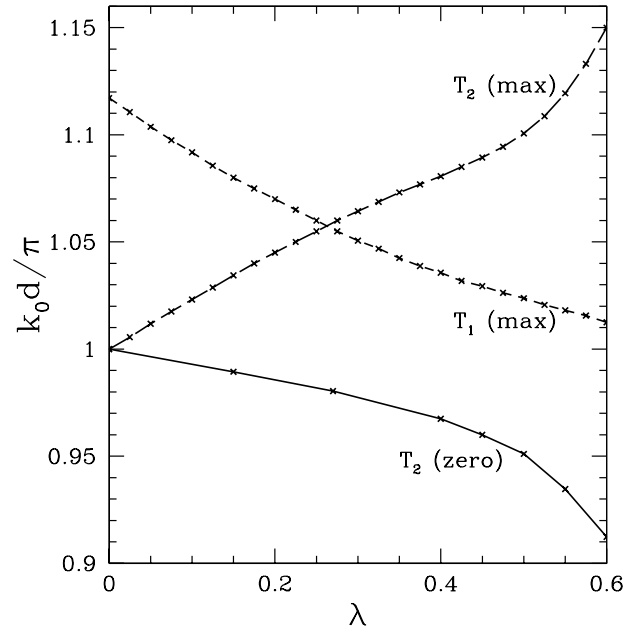


FIG. 10. The momentum k_0d/π or k_cd/π where T_1 (T_2) has its maximum (respectively zero and maximum) relative spectral weight graphed versus λ .

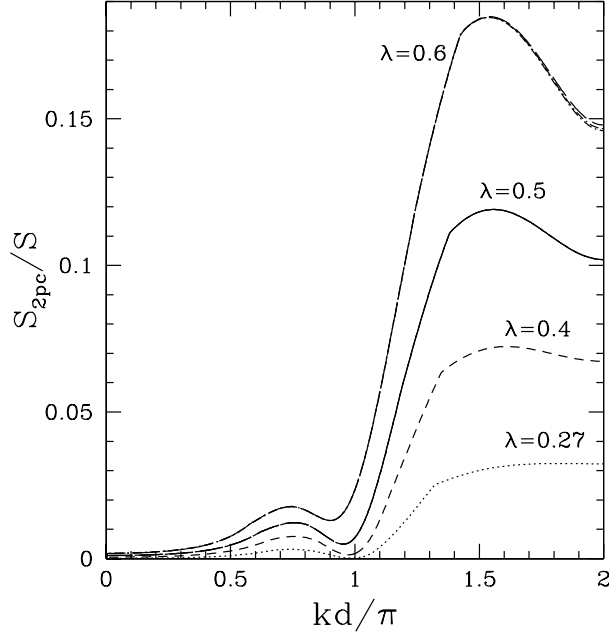


FIG. 11. The relative weight for the 2-particle continuum (S_{2pc}/S) for $\lambda = 0.27, 0.4, 0.5, 0.6$. The results of the three highest orders are plotted.

D. Complete Dynamical Structure Factor

The complete dynamical structure factor for $\lambda = 0.27$ was presented in our earlier paper [23]. The dynamical structure factor for the 2-particle continuum at $\lambda = 0.5$ is given in Fig. 12. A notable feature is the spike which develops as a bound state enters the continuum, discussed more fully in Ref. [23]. We will be happy to provide the complete dynamical structure factor for the AHC model for any value of λ , if requested.

Given the structure factor, one can also compute, for 2-particle states, the energy centroid $\langle\omega\rangle$ and the width $\Delta\omega$ which are defined as

$$\langle\omega\rangle = \frac{\int S_2(\omega, k) \omega d\omega}{\int S_2(\omega, k) d\omega} \quad (49)$$

$$\Delta\omega = \langle\omega^2\rangle - \langle\omega\rangle^2 \quad (50)$$

where $S_2(\omega, k)$ is the structure factor of the 2-particle states, including both the 2-particle bound states and 2-particle continuum. These quantities can be extracted readily from experiments. Our results are given in Figures 13 and 14 for various λ . We can see that $\Delta\omega$ has a nonzero minimum near $kd = \pi$, reflecting the presence of strong 2-particle bound states and a weak and narrow 2-particle continuum.

E. Auto-correlation function

Finally, we discuss the results for the spin auto-correlation functions. First, let us discuss the critical behaviour as $\lambda \rightarrow 1$. Schmidt and Uhrig [31] argued that the critical behaviour for the total auto correlation function (summed over ω) of the 1-particle state Φ_{1p} and 2-particle states Φ_{2p} should be

$$\Phi_{1p} \propto (1 - \lambda)^{1/3} \quad (51)$$

$$\Phi_{2p} \propto \text{const.} + O((1 - \lambda)^{1/3}) \quad (52)$$

modulo logarithms, as for the structure factors.

To verify these behaviours, we have applied Dlog Padé approximants to the series, and the results obtained from unbiased and biased Dlog Padé approximants are shown in Table IV. For Φ_{1p} , the results are consistent with Eq.

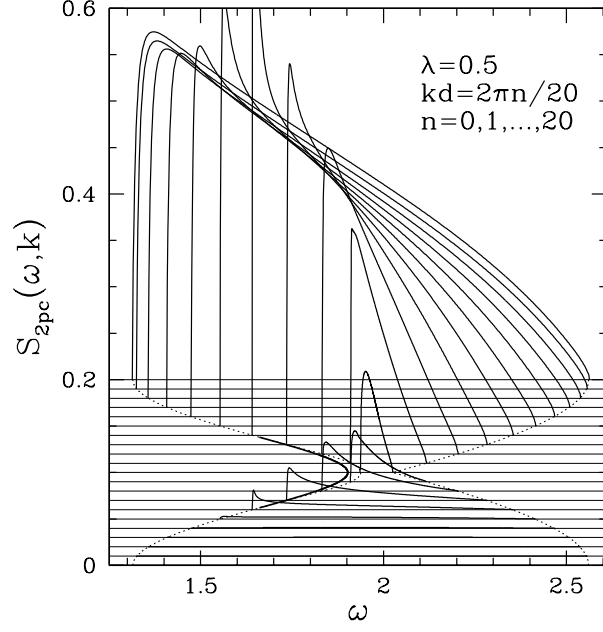


FIG. 12. The structure factor (shifted by $n/100$) for the 2-particle continuum versus energy ω at $\lambda = 0.5$ and $kd = 2\pi n/20$, $n = 0, 1, 2, \dots, 20$. Also shown as a bold solid line is the dispersion relation for the triplet bound-state T_1 .

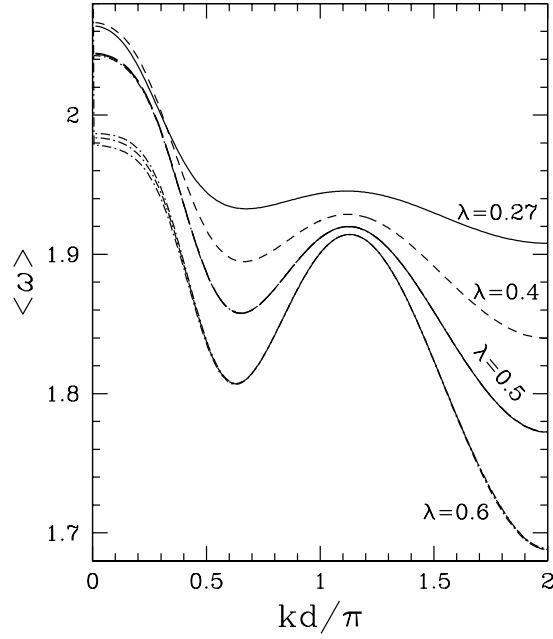


FIG. 13. The 2-particle energy centroid $\langle \omega \rangle$ versus k for $\lambda = 0.27, 0.4, 0.5, 0.6$.

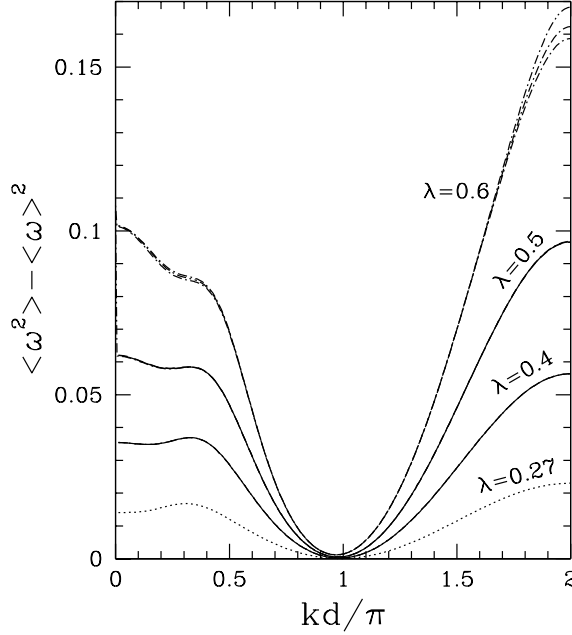


FIG. 14. The 2-particle width $\langle \omega^2 \rangle - \langle \omega \rangle^2$ versus k for $\lambda = 0.27, 0.4, 0.5, 0.6$.

(51). Assuming this behaviour, we can estimate the prefactor using integrated differential approximants. The result is

$$\Phi_{1p} = 1.258(2)(1 - \lambda)^{1/3} \quad (53)$$

For Φ_{2p} , however, the results are more ambiguous. The unbiased Dlog Padé approximants to $\partial\Phi_{2p}/\partial\lambda$ tend to exhibit defects for $\lambda < 1$, and the biased critical index for $\partial\Phi_{2p}/\partial\lambda$ is about -0.6, slightly smaller than -2/3. This might be due to an extra logarithmic correction.

The various auto-correlation functions versus λ are shown in Fig. 15, where one can see that Φ_{1p} vanishes at the limit $\lambda = 1$, while $(1 - \lambda)^{-1/3}\Phi_{1p}$ increases almost linearly as λ increases. The curve for $(\Phi_{1p} + \Phi_{2p})$, if we *assume* it is non-singular at $\lambda = 1$ (i.e. the singularities in Φ_{1p} and Φ_{2p} cancel exactly), runs almost flat with λ once we neglect unphysical and defective approximants: that would indicate that the 2-particle sector accounts for about 99.8% of the weight, even at $\lambda = 1$, which agrees almost exactly with the conclusions of Schmidt and Uhrig [31]. Remarkably, this is much higher than the fraction of 73% for the two-spinon continuum at $\lambda = 1$ calculated by Karbach *et al.* [35] from the exact solution. The result that sectors with more than 2 particles account for very little weight can be further understood from Fig. 7, where we can see that the remaining spectral weight near $kd = 2\pi$ for states of more than 2-particles actually decreases with λ , for large λ . Also shown in Fig. 15 is the direct extrapolation of the 2-particle auto-correlation Φ_{2p} using integrated differential approximants. These extrapolations assume that there is *no* singularity in Φ_{2p} at $\lambda = 1$, and the results give a somewhat smaller value of about 0.9 at $\lambda = 1$. For the bound states, the auto correlation function for T_2 increases, and reaches its maximum around $\lambda = 0.6$, then decreases, while the auto correlation function for T_1 continues to increase as far as we can follow it. We presume that Φ_{T_1} will also vanish as $\lambda \rightarrow 1$.

The autocorrelation function for the 2-particle continuum ($\Phi_{2pc}(\omega)$) is shown for various λ in Figure 16. The major feature is a spike at $\omega \sim 2$ which becomes more prominent as λ increases. This spike is due to contributions from the region around $kd = \pi$ near the lower threshold of the dispersion curve. It becomes divergent as $\lambda \rightarrow 1$, and matches rather neatly with a logarithmic divergence at $\omega = \pi/2$ discovered in the 2-spinon continuum by Karbach *et al.* [35]. Unfortunately, we can not compute an explicit series for $\Phi_{2pc}(\omega)$, so no series extrapolation can be made here.

Figure 16 also displays another small cusp or spike at lower ω , which occurs at the threshold energy where the triplet bound state T_1 merges with the continuum, i.e. where the structure factor diverges as shown in Figure 12. This position is marked by the arrow in Figure 16, for the case $\lambda = 0.6$. As $\lambda \rightarrow 1$, the T_1 threshold migrates towards $\omega = 0$, and the logarithmic divergence there [35] at $\lambda = 1$ may be viewed as relic of the T_1 bound state.

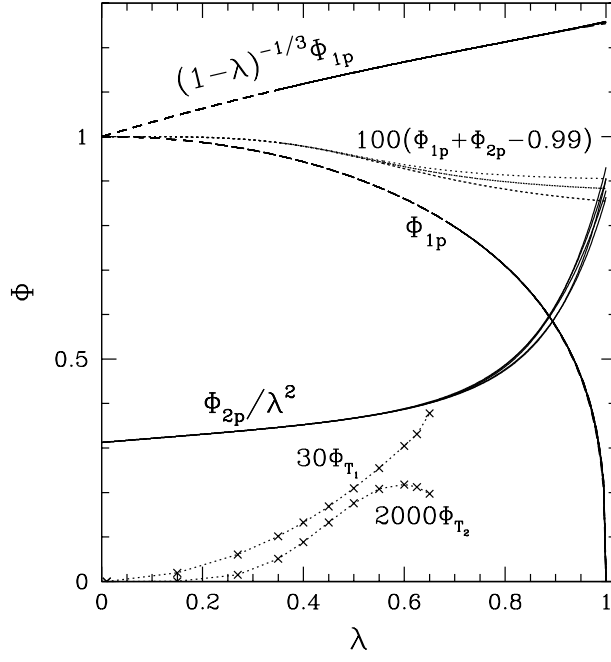


FIG. 15. The auto correlation functions versus λ for the 1-particle state (Φ_{1p}), 2-particle states (Φ_{2p}), and two particle bound states T_1 and T_2 .

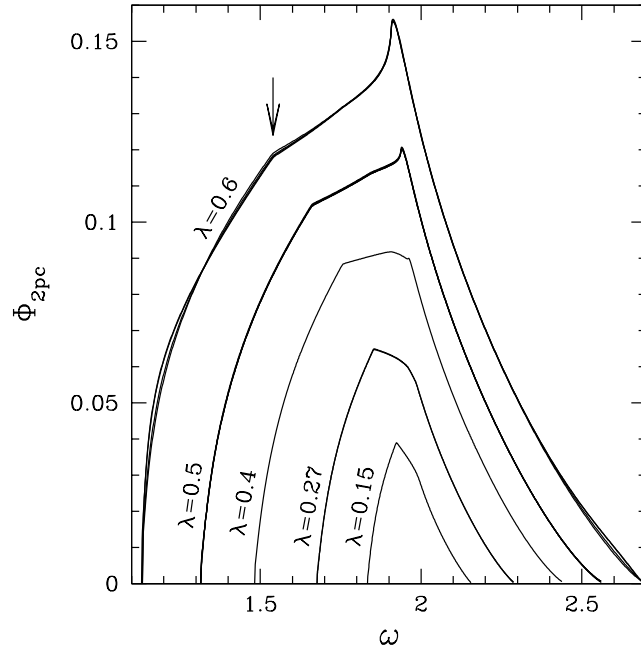


FIG. 16. The auto correlation function versus energy ω for the 2-particle continuum ($\Phi_{2pc}(\omega)$) for $\lambda = 0.15, 0.27, 0.4, 0.5, 0.6$.

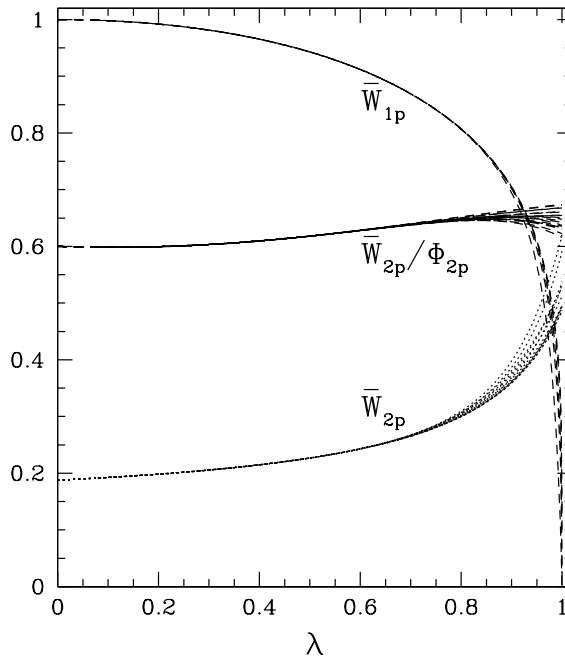


FIG. 17. The average weights (\overline{W}_{1p} and \overline{W}_{2p}) for 1 and 2 particle states, and ratio $\overline{W}_{2p}/\Phi_{2p}$ versus λ . Several different integrated differential approximants to the series are shown.

Note that the structure factor is dominated for $\lambda \rightarrow 1$ by $kd = 2\pi$, and so is the auto-correlation function. To get an idea of the multiparticle contributions to the dynamical structure factor at all wavevectors, we define the *average* relative weight, for a particular state Λ , as

$$\overline{W}_{\Lambda} = \frac{1}{2\pi} \sum_{\omega} \int_0^{2\pi} \frac{S_{\Lambda}(k, \omega)}{S(k)} dk \quad (54)$$

The series for the average relative weight for 2-particle states is given in Table III, and graphed as function of λ in Figure 17. Once again, we see that the average weight for the 1-particle state drops to zero as $\lambda \rightarrow 1$. The average weight for the 2-particle states has a sharp increase near $\lambda = 1$ which makes it difficult to estimate the results at $\lambda = 1$, but the result for the ratio $\overline{W}_{2p}/\Phi_{2p}$ is quite flat. Hence one estimates that \overline{W}_{2p} remains substantial, at about 60%, as $\lambda \rightarrow 1$. This is smaller than Φ_{2p} , showing that multiparticle excitations are more important away from the antiferromagnetic wavevector $kd = 2\pi$.

A priori, one might have expected that the average weights for 1-particle states, 2-particle states, etc, would all tend to zero as $\lambda \rightarrow 1$, with all the weight moving into many-particle states. Instead of that, we find that the weight for the 2-particle continuum remains finite and large, comparable to or by some measures even greater than that of the 2-spinon continuum computed by Karbach *et al.* [35]

IV. CONCLUSIONS AND DISCUSSION

We have shown in this paper how to calculate multiparticle structure factors and spectral weights to high orders in perturbation theory using linked-cluster expansion techniques [1,2]. Applying these techniques to the case of the alternating Heisenberg chain, a detailed picture has been given of both the integrated structure factors, and the individual spectral weights for the 1-particle state, 2-particle bound states and 2-particle continuum as functions of wavevector k . Continuing the series by means of Padé approximants or integrated differential approximants, good convergence is obtained from $\lambda = 0$ right up to $\lambda = 1$. Hopefully, it should be possible to test these predictions against experiments in the near future [5,6].

The 1-particle energy gap and spectral weight at general momenta appear to vanish as $\lambda \rightarrow 1$, following the behaviour predicted by Cross and Fisher [11], and already confirmed numerically by Singh and Zheng [22]. This

would seem to confirm the general notion that the triplets no longer form elementary excitations for the system at $\lambda = 1$. However, the 2-triplet spectral weight remains finite in the uniform limit and, in fact, appears to form the major part of the total spectral weight [31]. Schmidt and Uhrig [31] already pointed out that indeed the 2-triplet states carry a larger portion of the total spectral weight than the 2-spinon states, calculated by Karbach *et al.* [35]. We also find that the 2-particle auto-correlation functions for triplets display singularities similar to the known singularities for spinons [35].

We find that clear precursors to many features of the two-spinon continuum for the Heisenberg model, such as vanishing weight at the upper end of the continuum, divergent weight at the lower end of the continuum, cusps in the autocorrelation function, *etc.*, are already evident in the two-triplet continuum of the alternating chain. We have discovered an interesting result in that the logarithmic divergences at $\omega = 0$ in the auto correlation function of the uniform chain appears to be a relic of the triplet bound state T_1 in the non-uniform chain. Our highly accurate calculations of frequency and wavevector resolved spectral-weights should prove useful in understanding the spectral functions of real materials.

The crossover from elementary triplets to spin-half elementary excitations is quite different here than in the case of the $J_1 - J_2 - \delta$ model with $J_2/J_1 > 0.24$, where the uniform limit stays spontaneously dimerized. Affleck *et al* [13] presented the following picture in the latter case. The mass gap decreases exponentially as the uniform limit is approached, and in that limit the low-lying spectrum consists of a gapless continuum of soliton-antisoliton states. Away from the uniform limit, the soliton-antisoliton states are confined by a linear potential, giving rise to a ladder of discrete states, which correspond to the triplet excitations and their bound states. In the triplet language, on the other hand, the triplet energy gap drops to zero as the uniform limit is approached, and the multi-triplet bound states condense to form a continuum matching the soliton-antisoliton description. Numerical evidence confirms this picture [13,10].

The scenario appears to be quite different in the present case, where there is no next-nearest-neighbour interaction (J_2). Here the dimerization interaction has dimension $\frac{1}{2}$, giving rise to a gap which vanishes as $\delta^{2/3}$ in the uniform limit. In the soliton language [36], at small but non-zero δ , the low-lying spectrum consists of a soliton, an antisoliton, and a soliton-antisoliton bound state, forming a degenerate triplet, plus just one other soliton-antisoliton state at $\sqrt{3}$ times the mass. Since the soliton and antisoliton are not confined, a soliton-antisoliton continuum occurs at higher energy. In the triplet language, the 1-particle triplet corresponds to the three degenerate states, and the singlet bound state corresponds to the higher-lying one. There is no condensation of multi-triplet bound states; instead, the 2-triplet continuum drops down to match the spinon-antispinon continuum. The mass and spectral weight of the 1-triplet state vanishes as the uniform limit is approached; and naively one might expect the same to happen for the 2-triplet, 3-triplet states, etc, leaving many-triplet states to correspond to the spinon-antispinon continuum. Instead, we have found that the 2-triplet states dominate the total weight in the uniform limit, in agreement with Schmidt and Uhrig [31]. This is a peculiar and paradoxical feature, which argues that the triplet description remains at least as relevant as the spinon description, even in the uniform limit. The multi-triplet states ($n > 2$) still appear to carry only a tiny fraction of the spectral weight at $\lambda = 1$.

These findings call for further theoretical interpretation. Karbach *et al.* [37] have described the uniform Heisenberg antiferromagnet in terms of three different elementary excitations - magnons, spinons, and ‘psinons’ - each of which can be useful in different circumstances. None of these correspond to our dimer triplet excitations, however. Our work shows that a conventional picture, built as a perturbation around a trivial limit, can provide a highly accurate quantitative description of the system, when carried out to high orders.

ACKNOWLEDGMENTS

This work is supported in part by a grant from the Australian Research Council and the US National Science Foundation grant number DMR-0240918. We have benefited from discussions with Professor O.P. Sushkov and Professor J. Oitmaa. The computation has been performed on the AlphaServer SC computer. We are grateful for the computing resources provided by the Australian Partnership for Advanced Computing (APAC) National Facility.

* Email address: c.hamer@unsw.edu.au

[†] Email address: w.zheng@unsw.edu.au

- [1] S. Trebst, H. Monien, C.J. Hamer, W. Zheng, R.R.P. Singh, Phys. Rev. Lett. **85**, 4373 (2000).
- [2] W. Zheng, C.J. Hamer, R.R.P. Singh, S. Trebst, H. Monien, Phys. Rev. **B63**, 144410 (2001).
- [3] C. Knetter, K.P. Schmidt, M. Grüninger and G.S. Uhrig, Phys. Rev. Lett. **87**, 167204 (2001).
- [4] M.P. Gelfand and R.R.P. Singh, Adv. Phys. **49**, 93(2000).
- [5] G. Xu, C. Broholm, D.H. Reich and M.A. Adams, Phys. Rev. Lett. **84**, 4465 (2000).
- [6] D.A. Tennant, C. Broholm, D.H. Reich, S.E. Nagler, G.E. Granroth, T. Barnes, K. Damle, G. Xu, Y. Chen and B.C. Sales, cond-mat/0207678
- [7] G.S. Uhrig and H.J. Schulz, Phys. Rev. **B54**, R9624 (1996).
- [8] G. Bouzerar, A.P. Kampf and G.I. Japaridze, Phys. Rev. **58**, 3117 (1998).
- [9] A. Fledderjohann and C. Gros, Eur. Phys. Lett. **37**, 189 (1997).
- [10] W. Zheng, C.J. Hamer, R.R.P. Singh, S. Trebst, H. Monien, Phys. Rev. **B63**, 144411 (2001).
- [11] M.P.M. den Nijs, Physica **95A**, 449 (1979). M.C. Cross and D. Fisher, Phys. Rev. **B19**, 402 (1979). J.L. Black and V.J. Emery, Phys. Rev. **B23**, 429 (1981).
- [12] G.S. Uhrig, F. Schöfeld, M. Laukamp and E. Dagotto, Eur. Phys. J. **B7**, 67 (1999). T. Papenbrock, T. Barnes, D.J. Dean, M.V. Stoitsev and M.R. Stayer, cond-mat/0212254.
- [13] E.S. Sorenson, I. Affleck, D. Augier and D. Poilblanc, Phys. Rev. **B58**, R14701 (1998). I. Affleck, in *Dynamical Properties of Unconventional Magnetic Systems* (NATO ASI, Geilo, Norway, 1997).
- [14] W. Marshall and S.W. Lovesey, *Thermal Neutron Scattering* (Clarendon, Oxford, 1971).
- [15] T. Barnes, J. Riera and D.A. Tennant, Phys. Rev. **B59**, 11384 (1999).
- [16] A.C. Irving and C.J. Hamer, Nucl. Phys. **B230**, 361 (1984).
- [17] M.P. Gelfand, R.R.P. Singh and D.A. Huse, J. Stat. Phys. **59**, 1093 (1990).
- [18] H-X. He, C.J. Hamer and J. Oitmaa, J. Phys. **A23**, 1775 (1990).
- [19] M.P. Gelfand, Solid State Commun. **98**, 11 (1996).
- [20] R.R.P. Singh and M.P. Gelfand, Phys. Rev. **B52**, R15695(1995).
- [21] M.P. Gelfand, R.R.P. Singh and D.A. Huse, Phys. Rev. **B40**, 10801 (1989).
- [22] R.R.P. Singh and W. Zheng, Phys. Rev. **B59**, 9911 (1999).
- [23] W. Zheng, C.J. Hamer and R.R.P. Singh, cond-mat/0211346.
- [24] W. Duffy and K.P. Bair, Phys. Rev. **165**, 647 (1968).
- [25] J. Bonner and H.W.J. Blöte, Phys. Rev. **B25**, 6959 (1982).
- [26] X-F. Jiang, H. Chen and D.Y. Xing, J. Phys. **A34**, L259 (2001).
- [27] Z.G. Soos, S. Kuwajima and J.E. Mihalick, Phys. Rev. **B32**, 3124 (1985).
- [28] G. Spronken, B. Fourcade and Y. Lepine, Phys. Rev. **B33**, 1886 (1986).
- [29] T. Papenbrock, T. Barnes, D.J. Dean, M.V. Stoitsov and M.R. Strayer, cond-mat/0212254.
- [30] P. Shevchenko, V.N. Kotov and O.P. Sushkov, Phys. Rev. **B60**, 31305 (1999).
- [31] K.P. Schmidt, and G.S. Uhrig, Phys. Rev. Lett. **90**, 227204(2003).
- [32] M. Müller and H.J. Mikeska, cond-mat/0211335.
- [33] A.J. Guttmann, in “Phase Transitions and Critical Phenomena”, Vol. 13 ed. C. Domb and J. Lebowitz (New York, Academic, 1989).
- [34] I. Affleck, J. Phys. **A31**, 4573(1998).
- [35] M. Karbach, G. Müller, and A.H. Bougourzi, Phys. Rev. B **55**, 12510(1997).
- [36] R.F. Dashen, B. Hasslacher and A. Neveu, Phys. Rev. **D11**, 3423(1975).
- [37] M. Karbach, D. Biegel and G. Müller, cond-mat/0205142.

TABLE I. Series coefficients for the integrated structure factor $S(k) = \sum_{n,m} a_{n,m} \lambda^m \cos(nkd/2)$. Nonzero coefficients $a_{n,m}$ up to order $m = 13$ are listed.

(n, m)	$a_{n,m}$	(n, m)	$a_{n,m}$	(n, m)	$a_{n,m}$	(n, m)	$a_{n,m}$
(0, 0)	1.000000000	(4, 11)	$-1.591179666 \times 10^{-3}$	(9, 7)	$-2.661559650 \times 10^{-2}$	(15, 9)	$-9.209089311 \times 10^{-3}$
(1, 0)	-1.000000000	(4, 12)	$-1.346799079 \times 10^{-3}$	(9, 8)	$-1.701711998 \times 10^{-2}$	(15, 10)	$-1.132484677 \times 10^{-2}$
(1, 1)	$-2.500000000 \times 10^{-1}$	(4, 13)	$-1.135073475 \times 10^{-3}$	(9, 9)	$-1.047345923 \times 10^{-2}$	(15, 11)	$-1.152471081 \times 10^{-2}$
(1, 2)	$3.125000000 \times 10^{-2}$	(5, 2)	$-9.375000000 \times 10^{-2}$	(9, 10)	$-6.243270719 \times 10^{-3}$	(15, 12)	$-1.055798426 \times 10^{-2}$
(1, 3)	$2.864583333 \times 10^{-2}$	(5, 3)	$-1.119791667 \times 10^{-1}$	(9, 11)	$-3.511373171 \times 10^{-3}$	(15, 13)	$-9.126658607 \times 10^{-3}$
(1, 4)	$1.247829861 \times 10^{-3}$	(5, 4)	$-5.577256944 \times 10^{-2}$	(9, 12)	$-1.832316909 \times 10^{-3}$	(16, 8)	$1.534223557 \times 10^{-3}$
(1, 5)	$4.747178819 \times 10^{-4}$	(5, 5)	$-1.284450955 \times 10^{-2}$	(9, 13)	$-8.384814283 \times 10^{-4}$	(16, 9)	$4.630391871 \times 10^{-3}$
(1, 6)	$2.256346338 \times 10^{-3}$	(5, 6)	$1.543539542 \times 10^{-4}$	(10, 5)	$1.538085938 \times 10^{-2}$	(16, 10)	$7.630811251 \times 10^{-3}$
(1, 7)	$1.115188285 \times 10^{-3}$	(5, 7)	$2.104722325 \times 10^{-3}$	(10, 6)	$2.759165823 \times 10^{-2}$	(16, 11)	$9.315049401 \times 10^{-3}$
(1, 8)	$4.433909083 \times 10^{-4}$	(5, 8)	$2.590777271 \times 10^{-3}$	(10, 7)	$2.762316480 \times 10^{-2}$	(16, 12)	$9.630494889 \times 10^{-3}$
(1, 9)	$4.463708690 \times 10^{-4}$	(5, 9)	$2.541851515 \times 10^{-3}$	(10, 8)	$2.143434446 \times 10^{-2}$	(16, 13)	$9.064708700 \times 10^{-3}$
(1, 10)	$3.908585581 \times 10^{-4}$	(5, 10)	$2.142535125 \times 10^{-3}$	(10, 9)	$1.509559320 \times 10^{-2}$	(17, 8)	$-7.671117783 \times 10^{-4}$
(1, 11)	$2.721746108 \times 10^{-4}$	(5, 11)	$1.784799808 \times 10^{-3}$	(10, 10)	$1.026773209 \times 10^{-2}$	(17, 9)	$-2.828093400 \times 10^{-3}$
(1, 12)	$2.078935750 \times 10^{-4}$	(5, 12)	$1.526601703 \times 10^{-3}$	(10, 11)	$6.786844453 \times 10^{-3}$	(17, 10)	$-5.469609444 \times 10^{-3}$
(1, 13)	$1.752731379 \times 10^{-4}$	(5, 13)	$1.307569342 \times 10^{-3}$	(10, 12)	$4.357777095 \times 10^{-3}$	(17, 11)	$-7.545021498 \times 10^{-3}$
(2, 1)	$5.000000000 \times 10^{-1}$	(6, 3)	$7.812500000 \times 10^{-2}$	(10, 13)	$2.725607152 \times 10^{-3}$	(17, 12)	$-8.525536617 \times 10^{-3}$
(2, 2)	$6.250000000 \times 10^{-2}$	(6, 4)	$7.595486111 \times 10^{-2}$	(11, 5)	$-7.690429688 \times 10^{-3}$	(17, 13)	$-8.551663397 \times 10^{-3}$
(2, 3)	$-3.645833333 \times 10^{-2}$	(6, 5)	$3.919813368 \times 10^{-2}$	(11, 6)	$-1.887210799 \times 10^{-2}$	(18, 9)	$7.244944572 \times 10^{-4}$
(2, 4)	$-1.443142361 \times 10^{-2}$	(6, 6)	$1.485306540 \times 10^{-2}$	(11, 7)	$-2.397200110 \times 10^{-2}$	(18, 10)	$2.481638461 \times 10^{-3}$
(2, 5)	$-3.861038773 \times 10^{-3}$	(6, 7)	$5.066873213 \times 10^{-3}$	(11, 8)	$-2.190082988 \times 10^{-2}$	(18, 11)	$4.609868075 \times 10^{-3}$
(2, 6)	$-4.464373176 \times 10^{-3}$	(6, 8)	$1.200659217 \times 10^{-3}$	(11, 9)	$-1.703925617 \times 10^{-2}$	(18, 12)	$6.277698444 \times 10^{-3}$
(2, 7)	$-3.574776355 \times 10^{-3}$	(6, 9)	$-4.880865156 \times 10^{-4}$	(11, 10)	$-1.243639951 \times 10^{-2}$	(18, 13)	$7.142219966 \times 10^{-3}$
(2, 8)	$-2.152545002 \times 10^{-3}$	(6, 10)	$-1.061951430 \times 10^{-3}$	(11, 11)	$-8.818602901 \times 10^{-3}$	(19, 9)	$-3.622472286 \times 10^{-4}$
(2, 9)	$-1.614262178 \times 10^{-3}$	(6, 11)	$-1.168436483 \times 10^{-3}$	(11, 12)	$-6.103055681 \times 10^{-3}$	(19, 10)	$-1.483667264 \times 10^{-3}$
(2, 10)	$-1.364268756 \times 10^{-3}$	(6, 12)	$-1.145143702 \times 10^{-3}$	(11, 13)	$-4.131112380 \times 10^{-3}$	(19, 11)	$-3.187079773 \times 10^{-3}$
(2, 11)	$-1.085128141 \times 10^{-3}$	(6, 13)	$-1.075193082 \times 10^{-3}$	(12, 6)	$7.049560547 \times 10^{-3}$	(19, 12)	$-4.863723272 \times 10^{-3}$
(2, 12)	$-8.633290964 \times 10^{-4}$	(7, 3)	$-3.906250000 \times 10^{-2}$	(12, 7)	$1.552691676 \times 10^{-2}$	(19, 13)	$-6.030015201 \times 10^{-3}$
(2, 13)	$-7.178656848 \times 10^{-4}$	(7, 4)	$-6.331380208 \times 10^{-2}$	(12, 8)	$1.896538987 \times 10^{-2}$	(20, 10)	$3.441348672 \times 10^{-4}$
(3, 1)	$-2.500000000 \times 10^{-1}$	(7, 5)	$-4.956506800 \times 10^{-2}$	(12, 9)	$1.764401420 \times 10^{-2}$	(20, 11)	$1.318864692 \times 10^{-3}$
(3, 2)	$-1.875000000 \times 10^{-1}$	(7, 6)	$-2.639009923 \times 10^{-2}$	(12, 10)	$1.446797193 \times 10^{-2}$	(20, 12)	$2.724516711 \times 10^{-3}$
(3, 3)	$-2.343750000 \times 10^{-2}$	(7, 7)	$-1.199321708 \times 10^{-2}$	(12, 11)	$1.121713674 \times 10^{-2}$	(20, 13)	$4.090782507 \times 10^{-3}$
(3, 4)	$2.012803819 \times 10^{-2}$	(7, 8)	$-5.185196227 \times 10^{-3}$	(12, 12)	$8.435888979 \times 10^{-3}$	(21, 10)	$-1.720674336 \times 10^{-4}$
(3, 5)	$1.035789207 \times 10^{-2}$	(7, 9)	$-1.776089397 \times 10^{-3}$	(12, 13)	$6.212068934 \times 10^{-3}$	(21, 11)	$-7.750395765 \times 10^{-4}$
(3, 6)	$4.805176346 \times 10^{-3}$	(7, 10)	$-8.192333266 \times 10^{-5}$	(13, 6)	$-3.524780273 \times 10^{-3}$	(21, 12)	$-1.829266700 \times 10^{-3}$
(3, 7)	$4.284713101 \times 10^{-3}$	(7, 11)	$6.216205777 \times 10^{-4}$	(13, 7)	$-1.010268412 \times 10^{-2}$	(21, 13)	$-3.055890338 \times 10^{-3}$
(3, 8)	$3.284367466 \times 10^{-3}$	(7, 12)	$8.737107987 \times 10^{-4}$	(13, 8)	$-1.511986766 \times 10^{-2}$	(22, 11)	$1.642461866 \times 10^{-4}$
(3, 9)	$2.260859277 \times 10^{-3}$	(7, 13)	$9.485913165 \times 10^{-4}$	(13, 9)	$-1.626035314 \times 10^{-2}$	(22, 12)	$6.962934102 \times 10^{-4}$
(3, 10)	$1.762829643 \times 10^{-3}$	(8, 4)	$3.417968750 \times 10^{-2}$	(13, 10)	$-1.465683078 \times 10^{-2}$	(22, 13)	$1.582696489 \times 10^{-3}$
(3, 11)	$1.451718673 \times 10^{-3}$	(8, 5)	$4.730902778 \times 10^{-2}$	(13, 11)	$-1.210970065 \times 10^{-2}$	(23, 11)	$-8.212309331 \times 10^{-5}$
(3, 12)	$1.173179929 \times 10^{-3}$	(8, 6)	$3.645070394 \times 10^{-2}$	(13, 12)	$-9.584599362 \times 10^{-3}$	(23, 12)	$-4.034250937 \times 10^{-4}$
(3, 13)	$9.595019662 \times 10^{-4}$	(8, 7)	$2.204519358 \times 10^{-2}$	(13, 13)	$-7.395426977 \times 10^{-3}$	(23, 13)	$-1.037148415 \times 10^{-3}$
(4, 2)	$1.875000000 \times 10^{-1}$	(8, 8)	$1.249375691 \times 10^{-2}$	(14, 7)	$3.273010254 \times 10^{-3}$	(24, 12)	$7.870129775 \times 10^{-5}$
(4, 3)	$1.041666667 \times 10^{-1}$	(8, 9)	$6.866897220 \times 10^{-3}$	(14, 8)	$8.544238997 \times 10^{-3}$	(24, 13)	$3.656570992 \times 10^{-4}$
(4, 4)	$1.909722222 \times 10^{-2}$	(8, 10)	$3.496121257 \times 10^{-3}$	(14, 9)	$1.227229300 \times 10^{-2}$	(25, 12)	$-3.935064888 \times 10^{-5}$
(4, 5)	$-3.906250000 \times 10^{-3}$	(8, 11)	$1.579388581 \times 10^{-3}$	(14, 10)	$1.322238413 \times 10^{-2}$	(25, 13)	$-2.093578942 \times 10^{-4}$
(4, 6)	$-3.848888256 \times 10^{-3}$	(8, 12)	$5.538137269 \times 10^{-4}$	(14, 11)	$1.227668397 \times 10^{-2}$	(26, 13)	$3.783716238 \times 10^{-5}$
(4, 7)	$-3.145002043 \times 10^{-3}$	(8, 13)	$4.738508965 \times 10^{-6}$	(14, 12)	$1.055795986 \times 10^{-2}$	(27, 13)	$-1.891858119 \times 10^{-5}$
(4, 8)	$-2.985769420 \times 10^{-3}$	(9, 4)	$-1.708984375 \times 10^{-2}$	(14, 13)	$8.705553180 \times 10^{-3}$		
(4, 9)	$-2.431829046 \times 10^{-3}$	(9, 5)	$-3.485333478 \times 10^{-2}$	(15, 7)	$-1.636505127 \times 10^{-3}$		
(4, 10)	$-1.912181882 \times 10^{-3}$	(9, 6)	$-3.606061582 \times 10^{-2}$	(15, 8)	$-5.362708709 \times 10^{-3}$		

TABLE II. Series coefficients for the exclusive structure factors of the 1-particle triplet state $S_{1p}(k)$ $S_{1p}(k) = \sum_{n,m} a_{n,m} \lambda^m \cos(nkd/2)$. Nonzero coefficients $a_{n,m}$ up to order $m = 13$ are listed.

(n, m)	$a_{n,m}$	(n, m)	$a_{n,m}$	(n, m)	$a_{n,m}$	(n, m)	$a_{n,m}$
(0, 0)	1.000000000	(4, 2)	$1.875000000 \times 10^{-1}$	(8, 11)	$-6.011492935 \times 10^{-3}$	(14, 13)	$8.674883160 \times 10^{-3}$
(0, 2)	$-3.125000000 \times 10^{-1}$	(4, 3)	$1.458333333 \times 10^{-1}$	(8, 12)	$9.711804995 \times 10^{-3}$	(15, 7)	$-1.636505127 \times 10^{-3}$
(0, 3)	$-9.375000000 \times 10^{-2}$	(4, 4)	$6.835937500 \times 10^{-3}$	(8, 13)	$4.710318350 \times 10^{-3}$	(15, 8)	$-5.358020138 \times 10^{-3}$
(0, 4)	$1.627604167 \times 10^{-2}$	(4, 5)	$-5.485930266 \times 10^{-2}$	(9, 4)	$-1.708984375 \times 10^{-2}$	(15, 9)	$-9.241334017 \times 10^{-3}$
(0, 5)	$-8.257378472 \times 10^{-2}$	(4, 6)	$9.334422924 \times 10^{-3}$	(9, 5)	$-3.543203848 \times 10^{-2}$	(15, 10)	$-1.131045012 \times 10^{-2}$
(0, 6)	$-4.077148438 \times 10^{-2}$	(4, 7)	$7.197318057 \times 10^{-3}$	(9, 6)	$-3.456574899 \times 10^{-2}$	(15, 11)	$-1.142877596 \times 10^{-2}$
(0, 7)	$1.841892038 \times 10^{-2}$	(4, 8)	$-5.832889946 \times 10^{-2}$	(9, 7)	$-2.518777141 \times 10^{-2}$	(15, 12)	$-1.046099406 \times 10^{-2}$
(0, 8)	$-4.383319893 \times 10^{-2}$	(4, 9)	$-1.281724218 \times 10^{-2}$	(9, 8)	$-1.987998380 \times 10^{-2}$	(15, 13)	$-9.327327593 \times 10^{-3}$
(0, 9)	$-3.392954635 \times 10^{-2}$	(4, 10)	$2.152346878 \times 10^{-2}$	(9, 9)	$-1.377372682 \times 10^{-2}$	(16, 8)	$1.534223557 \times 10^{-3}$
(0, 10)	$1.671238124 \times 10^{-2}$	(4, 11)	$-4.067856177 \times 10^{-2}$	(9, 10)	$-1.514186704 \times 10^{-3}$	(16, 9)	$4.632624525 \times 10^{-3}$
(0, 11)	$-2.402930407 \times 10^{-2}$	(4, 12)	$-2.401466656 \times 10^{-2}$	(9, 11)	$-2.640524172 \times 10^{-4}$	(16, 10)	$7.616553597 \times 10^{-3}$
(0, 12)	$-3.094915187 \times 10^{-2}$	(4, 13)	$2.523955463 \times 10^{-2}$	(9, 12)	$-8.667418864 \times 10^{-3}$	(16, 11)	$9.310862860 \times 10^{-3}$
(0, 13)	$1.317777693 \times 10^{-2}$	(5, 2)	$-9.375000000 \times 10^{-2}$	(9, 13)	$-3.106212436 \times 10^{-4}$	(16, 12)	$9.677973448 \times 10^{-3}$
(1, 0)	-1.000000000	(5, 3)	$-1.223958333 \times 10^{-1}$	(10, 5)	$1.538085938 \times 10^{-2}$	(16, 13)	$9.174113955 \times 10^{-3}$
(1, 1)	$-2.500000000 \times 10^{-1}$	(5, 4)	$-4.031032986 \times 10^{-2}$	(10, 6)	$2.725408107 \times 10^{-2}$	(17, 8)	$-7.671117783 \times 10^{-4}$
(1, 2)	$5.000000000 \times 10^{-1}$	(5, 5)	$-1.652470341 \times 10^{-3}$	(10, 7)	$2.832565779 \times 10^{-2}$	(17, 9)	$-2.828986461 \times 10^{-3}$
(1, 3)	$1.432291667 \times 10^{-1}$	(5, 6)	$-2.680371131 \times 10^{-2}$	(10, 8)	$2.311140563 \times 10^{-2}$	(17, 10)	$-5.461641059 \times 10^{-3}$
(1, 4)	$-3.797743056 \times 10^{-2}$	(5, 7)	$-2.120727570 \times 10^{-3}$	(10, 9)	$1.449731923 \times 10^{-2}$	(17, 11)	$-7.554290412 \times 10^{-3}$
(1, 5)	$1.475604022 \times 10^{-1}$	(5, 8)	$3.677335722 \times 10^{-2}$	(10, 10)	$6.246098908 \times 10^{-3}$	(17, 12)	$-8.549734505 \times 10^{-3}$
(1, 6)	$6.164414206 \times 10^{-2}$	(5, 9)	$-4.177481543 \times 10^{-3}$	(10, 11)	$6.405727927 \times 10^{-3}$	(17, 13)	$-8.565778023 \times 10^{-3}$
(1, 7)	$-4.571135603 \times 10^{-2}$	(5, 10)	$-1.510927532 \times 10^{-2}$	(10, 12)	$8.071629661 \times 10^{-3}$	(18, 9)	$7.244944572 \times 10^{-4}$
(1, 8)	$7.541900211 \times 10^{-2}$	(5, 11)	$3.391969899 \times 10^{-2}$	(10, 13)	$-1.769051814 \times 10^{-4}$	(18, 10)	$2.481229141 \times 10^{-3}$
(1, 9)	$5.347557773 \times 10^{-2}$	(5, 12)	$1.090426758 \times 10^{-2}$	(11, 5)	$-7.690429688 \times 10^{-3}$	(18, 11)	$4.613304272 \times 10^{-3}$
(1, 10)	$-4.190407427 \times 10^{-2}$	(5, 13)	$-2.101789738 \times 10^{-2}$	(11, 6)	$-1.875154472 \times 10^{-2}$	(18, 12)	$6.275948659 \times 10^{-3}$
(1, 11)	$3.910767511 \times 10^{-2}$	(6, 3)	$7.812500000 \times 10^{-2}$	(11, 7)	$-2.441788701 \times 10^{-2}$	(18, 13)	$7.129091829 \times 10^{-3}$
(1, 12)	$5.118486369 \times 10^{-2}$	(6, 4)	$6.727430556 \times 10^{-2}$	(11, 8)	$-2.218640450 \times 10^{-2}$	(19, 9)	$-3.622472286 \times 10^{-4}$
(1, 13)	$-3.356079789 \times 10^{-2}$	(6, 5)	$4.458279080 \times 10^{-2}$	(11, 9)	$-1.605467746 \times 10^{-2}$	(19, 10)	$-1.483499815 \times 10^{-3}$
(2, 1)	$5.000000000 \times 10^{-1}$	(6, 6)	$3.504162070 \times 10^{-2}$	(11, 10)	$-1.111541180 \times 10^{-2}$	(19, 11)	$-3.188966289 \times 10^{-3}$
(2, 2)	$-1.250000000 \times 10^{-1}$	(6, 7)	$2.109803094 \times 10^{-3}$	(11, 11)	$-1.034165700 \times 10^{-2}$	(19, 12)	$-4.859982468 \times 10^{-3}$
(2, 3)	$-2.604166667 \times 10^{-2}$	(6, 8)	$-1.579822777 \times 10^{-2}$	(11, 12)	$-8.030332288 \times 10^{-3}$	(19, 13)	$-6.025154806 \times 10^{-3}$
(2, 4)	$1.779513889 \times 10^{-2}$	(6, 9)	$1.297988287 \times 10^{-2}$	(11, 13)	$-1.448277762 \times 10^{-3}$	(20, 10)	$3.441348672 \times 10^{-4}$
(2, 5)	$-1.206416377 \times 10^{-1}$	(6, 10)	$6.764275332 \times 10^{-3}$	(12, 6)	$7.049560547 \times 10^{-3}$	(20, 11)	$1.318939114 \times 10^{-3}$
(2, 6)	$-2.833321654 \times 10^{-2}$	(6, 11)	$-2.652577291 \times 10^{-2}$	(12, 7)	$1.559121717 \times 10^{-2}$	(20, 12)	$2.723720941 \times 10^{-3}$
(2, 7)	$4.500562644 \times 10^{-2}$	(6, 12)	$-1.873115433 \times 10^{-3}$	(12, 8)	$1.875765450 \times 10^{-2}$	(20, 13)	$4.091885849 \times 10^{-3}$
(2, 8)	$-6.561594063 \times 10^{-2}$	(6, 13)	$1.362791590 \times 10^{-2}$	(12, 9)	$1.728643232 \times 10^{-2}$	(21, 10)	$-1.720674336 \times 10^{-4}$
(2, 9)	$-3.427604879 \times 10^{-2}$	(7, 3)	$-3.906250000 \times 10^{-2}$	(12, 10)	$1.481153271 \times 10^{-2}$	(21, 11)	$-7.750705856 \times 10^{-4}$
(2, 10)	$4.545736434 \times 10^{-2}$	(7, 4)	$-6.070963542 \times 10^{-2}$	(12, 11)	$1.267199966 \times 10^{-2}$	(21, 12)	$-1.828835480 \times 10^{-3}$
(2, 11)	$-3.409665942 \times 10^{-2}$	(7, 5)	$-5.429642289 \times 10^{-2}$	(12, 12)	$8.696286848 \times 10^{-3}$	(21, 13)	$-3.057141912 \times 10^{-3}$
(2, 12)	$-3.879019409 \times 10^{-2}$	(7, 6)	$-3.120500070 \times 10^{-2}$	(12, 13)	$4.298281913 \times 10^{-3}$	(22, 11)	$1.642461866 \times 10^{-4}$
(2, 13)	$3.772049749 \times 10^{-2}$	(7, 7)	$-3.188448384 \times 10^{-3}$	(13, 6)	$-3.524780273 \times 10^{-3}$	(22, 12)	$6.962799729 \times 10^{-4}$
(3, 1)	$-2.500000000 \times 10^{-1}$	(7, 8)	$1.279329754 \times 10^{-3}$	(13, 7)	$-1.012679677 \times 10^{-2}$	(22, 13)	$1.582874937 \times 10^{-3}$
(3, 2)	$-1.562500000 \times 10^{-1}$	(7, 9)	$-1.467444993 \times 10^{-2}$	(13, 8)	$-1.499607686 \times 10^{-2}$	(23, 11)	$-8.212309331 \times 10^{-5}$
(3, 3)	$-8.593750000 \times 10^{-2}$	(7, 10)	$-9.349685042 \times 10^{-4}$	(13, 9)	$-1.624052105 \times 10^{-2}$	(23, 12)	$-4.034194087 \times 10^{-4}$
(3, 4)	$1.372612847 \times 10^{-2}$	(7, 11)	$1.714891750 \times 10^{-2}$	(13, 10)	$-1.498198003 \times 10^{-2}$	(23, 13)	$-1.037244158 \times 10^{-3}$
(3, 5)	$1.005768953 \times 10^{-1}$	(7, 12)	$-5.294607061 \times 10^{-3}$	(13, 11)	$-1.252169240 \times 10^{-2}$	(24, 12)	$7.870129775 \times 10^{-5}$
(3, 6)	$9.286244710 \times 10^{-3}$	(7, 13)	$-8.581846951 \times 10^{-3}$	(13, 12)	$-9.049303257 \times 10^{-3}$	(24, 13)	$3.656595110 \times 10^{-4}$
(3, 7)	$-2.312368150 \times 10^{-2}$	(8, 4)	$3.417968750 \times 10^{-2}$	(13, 13)	$-6.457204366 \times 10^{-3}$	(25, 12)	$-3.935064888 \times 10^{-5}$
(3, 8)	$6.813065057 \times 10^{-2}$	(8, 5)	$4.904513889 \times 10^{-2}$	(14, 7)	$3.273010254 \times 10^{-3}$	(25, 13)	$-2.093589278 \times 10^{-4}$
(3, 9)	$2.664720824 \times 10^{-2}$	(8, 6)	$3.434541490 \times 10^{-2}$	(14, 8)	$8.532182670 \times 10^{-3}$	(26, 13)	$3.783716238 \times 10^{-5}$
(3, 10)	$-3.218290488 \times 10^{-2}$	(8, 7)	$1.559162061 \times 10^{-2}$	(14, 9)	$1.232853596 \times 10^{-2}$	(27, 13)	$-1.891858119 \times 10^{-5}$
(3, 11)	$4.070336366 \times 10^{-2}$	(8, 8)	$1.322605786 \times 10^{-2}$	(14, 10)	$1.328042130 \times 10^{-2}$		
(3, 12)	$3.466875907 \times 10^{-2}$	(8, 9)	$1.580418652 \times 10^{-2}$	(14, 11)	$1.213368398 \times 10^{-2}$		
(3, 13)	$-3.003621683 \times 10^{-2}$	(8, 10)	$9.329997203 \times 10^{-4}$	(14, 12)	$1.012086983 \times 10^{-2}$		

TABLE III. Series coefficients for the integrated structure factor $S(k)$, the exclusive 1-particle structure factor $S_{1p}(k)$, and the total 2-particle structure factor $S_{2p}(k)$ at $kd = \pi, 2\pi$, together with the structure factors ($S_{T_1}(k)$, $S_{T_2}(k)$, and $S_{2pc}(k)$) for 2-particle bound states T_1 and T_2 , and 2-particle continuum at $kd = \pi$, the auto correlation function of 1-particle (Φ_{1p}) and 2-particle states (Φ_{2p}), the average relative weight for 2-particle states (\overline{W}_{2p}), and R , R_{1p} , and R_{2p} . Series coefficients of λ^m up to order $m = 13$ are listed.

m	$S(\pi)$	$S_{1p}(\pi)$	$S_{2p}(\pi)$	$S_{T_1}(\pi)$	$S_{T_2}(\pi)$
0	1.000000000	1.000000000	0.000000000	0.000000000	0.000000000
1	$-5.000000000 \times 10^{-1}$	$-5.000000000 \times 10^{-1}$	0.000000000	0.000000000	0.000000000
2	$1.250000000 \times 10^{-1}$	0.000000000	$1.250000000 \times 10^{-1}$	$1.250000000 \times 10^{-1}$	0.000000000
3	$6.250000000 \times 10^{-2}$	0.000000000	$6.250000000 \times 10^{-2}$	$6.250000000 \times 10^{-2}$	0.000000000
4	$-8.246527778 \times 10^{-3}$	$-2.777777778 \times 10^{-2}$	$1.584201389 \times 10^{-2}$	$4.557291667 \times 10^{-3}$	$2.604166667 \times 10^{-3}$
5	$-7.315176505 \times 10^{-3}$	$-2.770996094 \times 10^{-2}$	$1.725260417 \times 10^{-2}$	$-2.365451389 \times 10^{-2}$	$5.642361111 \times 10^{-3}$
6	$1.671025782 \times 10^{-3}$	$-2.400457123 \times 10^{-2}$	$2.357124988 \times 10^{-2}$	$-6.690809462 \times 10^{-2}$	$4.643192998 \times 10^{-3}$
7	$2.038836381 \times 10^{-3}$	$-2.191502135 \times 10^{-2}$	$2.248861054 \times 10^{-2}$	$-1.295114399 \times 10^{-1}$	$-3.105917095 \times 10^{-3}$
8	$9.809032520 \times 10^{-4}$	$-1.887358236 \times 10^{-2}$	$1.753652230 \times 10^{-2}$	$-1.919116349 \times 10^{-1}$	$-1.721538889 \times 10^{-2}$
9	$7.194422822 \times 10^{-4}$	$-1.527772889 \times 10^{-2}$	$1.378672204 \times 10^{-2}$	$-2.252182500 \times 10^{-1}$	$-3.106542706 \times 10^{-2}$
10	$4.813229257 \times 10^{-4}$	$-1.228831810 \times 10^{-2}$	$1.083241128 \times 10^{-2}$	$-1.979558323 \times 10^{-1}$	$-3.789373385 \times 10^{-2}$
11	$2.551816973 \times 10^{-4}$	$-1.011208718 \times 10^{-2}$	$9.645537754 \times 10^{-3}$	$-7.313449239 \times 10^{-2}$	$-3.170664884 \times 10^{-2}$
12	$1.953605167 \times 10^{-4}$	$-8.576749497 \times 10^{-3}$	$7.501091661 \times 10^{-3}$	$1.758607061 \times 10^{-1}$	$-6.069523293 \times 10^{-3}$
13	$2.020270912 \times 10^{-4}$	$-7.538604157 \times 10^{-3}$	$7.444260493 \times 10^{-3}$	$5.577962015 \times 10^{-1}$	$4.352098881 \times 10^{-2}$
14					$1.144814294 \times 10^{-1}$
m	$S_{2pc}(\pi)$	$S(2\pi)$	$S_{1p}(2\pi)$	$S_{2p}(2\pi)$	Φ_{1p}
0	0.000000000	2.000000000	2.000000000	0.000000000	1.000000000
1	0.000000000	1.000000000	1.000000000	0.000000000	0.000000000
2	0.000000000	$5.000000000 \times 10^{-1}$	$-5.000000000 \times 10^{-1}$	1.000000000	$-3.125000000 \times 10^{-1}$
3	0.000000000	$2.916666667 \times 10^{-1}$	$2.083333333 \times 10^{-1}$	$8.333333333 \times 10^{-2}$	$-9.375000000 \times 10^{-2}$
4	$8.680555556 \times 10^{-3}$	$2.296006944 \times 10^{-1}$	$2.847222222 \times 10^{-1}$	$-9.027777778 \times 10^{-2}$	$1.627604167 \times 10^{-2}$
5	$3.526475694 \times 10^{-2}$	$1.882414641 \times 10^{-1}$	$-2.981318721 \times 10^{-1}$	$4.924768519 \times 10^{-1}$	$-8.257378472 \times 10^{-2}$
6	$8.583615150 \times 10^{-2}$	$1.552634534 \times 10^{-1}$	$8.784079846 \times 10^{-2}$	$1.213981723 \times 10^{-1}$	$-4.077148438 \times 10^{-2}$
7	$1.551059676 \times 10^{-1}$	$1.336307604 \times 10^{-1}$	$2.710263476 \times 10^{-1}$	$-1.130861384 \times 10^{-1}$	$1.841892038 \times 10^{-2}$
8	$2.266635461 \times 10^{-1}$	$1.180685972 \times 10^{-1}$	$-2.368294851 \times 10^{-1}$	$3.319204641 \times 10^{-1}$	$-4.383319893 \times 10^{-2}$
9	$2.700703991 \times 10^{-1}$	$1.053990124 \times 10^{-1}$	$-5.538722908 \times 10^{-3}$	$2.095799705 \times 10^{-1}$	$-3.392954635 \times 10^{-2}$
10	$2.466819774 \times 10^{-1}$	$9.514478385 \times 10^{-2}$	$2.723409199 \times 10^{-1}$	$3.264975567 \times 10^{-2}$	$1.671238124 \times 10^{-2}$
11	$1.144866790 \times 10^{-1}$	$8.684667562 \times 10^{-2}$	$-1.694460542 \times 10^{-1}$	$4.627752009 \times 10^{-1}$	$-2.402930407 \times 10^{-2}$
12	$-1.622900912 \times 10^{-1}$	$7.991574506 \times 10^{-2}$	$-7.914782458 \times 10^{-2}$	$4.466072907 \times 10^{-1}$	$-3.094915187 \times 10^{-2}$
13	$-5.938729299 \times 10^{-1}$	$7.400747491 \times 10^{-2}$	$2.593075729 \times 10^{-1}$	$7.243209793 \times 10^{-1}$	$1.317777693 \times 10^{-2}$
m	Φ_{2p}	\overline{W}_{2p}	$R = \lim_{k \rightarrow 0} S/k^2$	$R_{1p} = \lim_{k \rightarrow 0} S_{1p}/k^2$	$R_{2p} = \lim_{k \rightarrow 0} S_{2p}/k^2$
0	0.000000000	1.000000000	$1.250000000 \times 10^{-1}$	$1.250000000 \times 10^{-1}$	0.000000000
1	0.000000000	0.000000000	$6.250000000 \times 10^{-2}$	$6.250000000 \times 10^{-2}$	0.000000000
2	$3.125000000 \times 10^{-1}$	$-1.875000000 \times 10^{-1}$	$9.375000000 \times 10^{-2}$	$9.375000000 \times 10^{-2}$	0.000000000
3	$9.375000000 \times 10^{-2}$	$-4.687500000 \times 10^{-2}$	$7.031250000 \times 10^{-2}$	$7.031250000 \times 10^{-2}$	0.000000000
4	$-2.636718750 \times 10^{-2}$	$-3.103298611 \times 10^{-2}$	$6.610785590 \times 10^{-2}$	$6.141493056 \times 10^{-2}$	$4.448784722 \times 10^{-3}$
5	$8.148871528 \times 10^{-2}$	$-6.538447627 \times 10^{-2}$	$6.383938260 \times 10^{-2}$	$6.599765354 \times 10^{-2}$	$-2.305772569 \times 10^{-3}$
6	$5.053823966 \times 10^{-2}$	$-1.166864089 \times 10^{-2}$	$6.018220642 \times 10^{-2}$	$6.027503661 \times 10^{-2}$	$-1.646442178 \times 10^{-4}$
7	$-1.360771980 \times 10^{-2}$	$2.293814357 \times 10^{-3}$	$5.737893768 \times 10^{-2}$	$5.616068546 \times 10^{-2}$	$9.660760071 \times 10^{-4}$
8	$3.967389006 \times 10^{-2}$	$-3.920166318 \times 10^{-2}$	$5.536595911 \times 10^{-2}$	$5.331091464 \times 10^{-2}$	$1.625177465 \times 10^{-3}$
9	$5.235992915 \times 10^{-2}$	$-1.075891724 \times 10^{-2}$	$5.357448621 \times 10^{-2}$	$5.601825866 \times 10^{-2}$	$-3.020253684 \times 10^{-3}$
10	$1.907595256 \times 10^{-2}$	$7.139608316 \times 10^{-3}$	$5.194887667 \times 10^{-2}$	$5.101011394 \times 10^{-2}$	$-3.106958042 \times 10^{-5}$
11	$6.149786123 \times 10^{-2}$	$-2.797421962 \times 10^{-2}$	$5.053076987 \times 10^{-2}$	$4.803748655 \times 10^{-2}$	$6.937664269 \times 10^{-4}$
12	$7.568512290 \times 10^{-2}$	$-1.386098936 \times 10^{-2}$	$4.927953902 \times 10^{-2}$	$5.120296763 \times 10^{-2}$	$-5.289988311 \times 10^{-3}$
13	$1.267526913 \times 10^{-1}$	$9.053856936 \times 10^{-3}$	$4.815020988 \times 10^{-2}$	$4.831429881 \times 10^{-2}$	$-6.876775997 \times 10^{-3}$

TABLE IV. $[n/m]$ Dlog Padé approximants to the series for $\partial S^{2/3}/\partial\lambda$ and $\partial S^{4/5}/\partial\lambda$ at $kd = 2\pi$, for Φ_{1p} , and for $\partial\Phi_{2p}/\partial\lambda$. The position of the singularity (pole), the critical index (U.B.R.) from unbiased approximants, and the critical index from biased approximants (B.R.) are given. An asterisk denotes a defective approximant.

n	$[(n-2)/n]$ pole (N.B.R., B.R.)	$[(n-1)/n]$ pole (N.B.R., B.R.)	$[n/n]$ pole (N.B.R., B.R.)	$[(n+1)/n]$ pole (N.B.R., B.R.)	$[(n+2)/n]$ pole (N.B.R., B.R.)
$\partial S(2\pi)^{2/3}/\partial\lambda$					
n= 1			0.6244(-0.2599, -0.7844)	1.0859(-1.3670, -0.9980)	1.0837(-1.3560, -0.2298)
n= 2	* (* , -1.0983)	* (* , *)	1.0837(-1.3561, -0.9488)	* (* , -0.9530)	0.9694(-0.7956, -0.9621)
n= 3	* (* , -1.1246)	0.9952(-0.9312, -0.9534)	0.9895(-0.9048, -0.9449)	0.9933(-0.9257, -0.9802)	0.9974(-0.9523, -0.9747)
n= 4	0.9899(-0.9074, -0.9629)	0.9918(-0.9168, -0.9876)	* (* , -0.9738)	0.9981(-0.9582, -0.9765)	0.9980(-0.9576, -0.9300)
n= 5	* (* , -0.9764)	0.9970(-0.9483, -0.9773)	0.9980(-0.9575, -0.9821)	0.9981(-0.9581, -0.9832)	
n= 6	0.9981(-0.9586, -0.9758)	0.9993(-0.9724, -0.9832)			
$\partial S(2\pi)^{4/5}/\partial\lambda$					
n= 1			0.6406(-0.2873, -0.8325)	1.0777(-1.3676, -1.0271)	1.0833(-1.3962, *)
n= 2	* (* , -1.0775)	0.8684(-0.6358, -1.2702)	1.0833(-1.3967, -0.9784)	1.0779(-1.3683, -0.9813)	0.9710(-0.8264, -0.9895)
n= 3	* (* , -1.1123)	0.9969(-0.9668, -0.9814)	0.9907(-0.9375, -0.9768)	0.9941(-0.9565, -1.0057)	0.9979(-0.9823, -1.0000)
n= 4	0.9913(-0.9406, -0.9898)	0.9930(-0.9494, -1.0134)	* (* , -0.9990)	0.9986(-0.9875, -1.0015)	0.9985(-0.9865, -0.9861)
n= 5	* (* , -1.0016)	0.9975(-0.9782, -1.0021)	0.9984(-0.9862, -1.0058)	0.9985(-0.9872, -1.0065)	
n= 6	0.9985(-0.9871, -1.0014)	0.9995(-0.9994, -1.0065)			
Φ_{1p}					
n= 1			* (* , 0.0118)	0.2328(0.0004, 0.2419)	* (* , 0.3983)
n= 2	* (* , 0.2984)	* (* , 0.3254)	0.6947(0.0613, 0.3328)	* (* , 0.3252)	* (* , 0.3231)
n= 3	0.9773(0.3025, 0.3354)	1.0250(0.3680, 0.3289)	1.0065(0.3359, 0.3224)	0.9901(0.3043, 0.3244)	0.9935(0.3117, 0.3327)
n= 4	1.0111(0.3449, 0.3250)	0.9266(0.1528, 0.3257)	0.9929(0.3103, 0.3269)	* (* , 0.3311)	0.9953(0.3162, 0.3323)
n= 5	0.9965(0.3188, 0.3215)	0.9954(0.3164, 0.3218)	0.9948(0.3148, 0.3187)	0.9952(0.3158, 0.3568)	
n= 6	* (* , 0.3215)	0.9951(0.3154, 0.3225)			
$\partial\Phi_{2p}/\partial\lambda$					
n= 1			-0.2374(0.0304, -0.1924)	* (* , -1.1986)	* (* , *)
n= 2	0.7175(-0.1129, -0.2521)	0.2556(-0.0140, -0.1334)	(* , -0.7531)	* (* , -0.7601)	* (* , *)
n= 3	0.4363(-0.0604, 0.0112)	0.9908(-0.7323, -0.7603)	0.7409(-0.2107, -0.7529)	0.6647(-0.1138, -0.4809)	0.5793(-0.0453, -0.6359)
n= 4	0.8362(-0.3880, -1.0869)	0.6399(-0.0869, -0.6158)	0.3412(-0.0003, -0.6030)	0.6184(-0.0724, -0.5041)	0.6071(-0.0630, -0.1906)
n= 5	0.4558(-0.0054, -0.6038)	0.5885(-0.0485, -0.6162)	0.6023(-0.0588, *)		
n= 6	0.6035(-0.0599, -0.4355)				